

Adversarial Bayesian Simulation

Yuexi Wang and Veronika Ročková
Booth School of Business, University of Chicago

July 24, 2023

Abstract

In the absence of explicit or tractable likelihoods, Bayesians often resort to approximate Bayesian computation (ABC) for inference. Our work bridges ABC with deep neural implicit samplers based on generative adversarial networks (GANs) and adversarial variational Bayes. Both ABC and GANs compare aspects of observed and fake data to simulate from posteriors and likelihoods, respectively. We develop a Bayesian GAN (B-GAN) sampler that directly targets the posterior by solving an adversarial optimization problem. B-GAN is driven by a deterministic mapping learned on the ABC reference by *conditional* GANs. Once the mapping has been trained, iid posterior samples are obtained by filtering noise at a negligible additional cost. We propose two post-processing local refinements using (1) data-driven proposals with importance reweighting, and (2) variational Bayes. We support our findings with frequentist-Bayesian results, showing that the typical total variation distance between the true and approximate posteriors converges to zero for certain neural network generators and discriminators. Our findings on simulated data show highly competitive performance relative to some of the most recent likelihood-free posterior simulators.

Keywords: Approximate Bayesian Computation; Generative Adversarial Networks; Implicit Models; Likelihood-free Bayesian Inference, Variational Bayes

1 ABC and Beyond

For a practitioner, much of the value of the Bayesian inferential approach hinges on the ability to compute the entire posterior distribution. Very often, it is easier to infer data-generating probability distributions through simulator models rather than likelihood functions. However, Bayesian computation with simulator models can be particularly grueling.

We assume that $\theta \in \Theta \subset \mathbb{R}^d$ is a parameter controlling a simulator-based model that gives rise to a data vector $X_\theta^{(n)} = (X_1, \dots, X_n)' \sim P_\theta^{(n)}$ which is *not* necessarily iid. The model may be provided by a probabilistic program that can be easily simulated but its implicit likelihood $p_\theta^{(n)} = \pi(X^{(n)} | \theta)$ cannot be evaluated. For an unknown inferential target $\theta_0 \in \Theta$, our goal is to approximate the post-data inferential density (i.e. the posterior)

$$\pi(\theta | X_0^{(n)}) \propto p_\theta^{(n)}(X_0^{(n)})\pi(\theta), \quad (1)$$

where $X_0^{(n)} \sim P_{\theta_0}^{(n)}$ denotes the observed data. We allow for the possibility that *both* the likelihood $p_\theta^{(n)}(\cdot)$ and/or the prior $\pi(\theta)$ are analytically intractable but easy to draw from.

Without the obligation to build a model, Approximate Bayesian Computation (ABC) (Beaumont et al., 2002; Sisson et al., 2018) provides an approximation to the posterior (1) by matching aspects of observed and fake data. This is accomplished via forward simulation of the so-called ABC reference table $\{(\theta_j, X_j^{(n)})\}_{j=1}^T$ where θ_j 's have been sampled from the prior $\pi(\theta)$ and fake data $X_j^{(n)}$'s have been sampled from the likelihood $p_{\theta_j}^{(n)}(\cdot)$. In order to keep only plausible parameter draws, this table is then filtered through an accept/reject mechanism to weed out parameter values θ_j for which the summary statistics of the fake and observed data were too far. Our work, albeit not being an ABC method per-se, builds off of recent ABC and simulation-based Bayesian inference innovations described below.

ABC Regression adjustment (Beaumont et al., 2002; Beaumont, 2003; Blum and François, 2010) is a post-processing step that re-weights and re-adjusts the location of θ_j 's gathered by rejection ABC by fitting a (weighted) regression model of θ_j 's onto summary statistics $s_j = s(X_j^{(n)})$. Such a model can be regarded as provisional density estimator of $\pi(\theta | X^{(n)})$ derived from $s(X^{(n)})$ under certain regression distributional assumptions. More flexible conditional density estimators, such as neural mixture density networks (Papamakarios and Murray, 2016; Lueckmann et al., 2017), have been successfully integrated into ABC without the burden of choosing summary statistics. Our approach is related to these developments. However, we do not attempt to learn a flexible parametric approximation to the posterior (or the likelihood (Lueckmann et al., 2019; Papamakarios et al., 2019)). Instead, we find an *implicit* neural sampler from an approximation to $\pi(\theta | X^{(n)})$ by training

Generative Adversarial Networks (Goodfellow et al., 2016) on the ABC reference table. GANs have been originally conceived to simulate from complex likelihoods by contrasting observed and fake data. ABC, on the other hand, contrasts observed and fake data to simulate from complex posteriors. Bringing together these two approaches, we propose the B-GAN posterior sampler, an incarnation of conditional GANs (Gauthier, 2014; Mirza and Osindero, 2014; Athey et al., 2021; Zhou et al., 2022) for likelihood-free Bayesian simulation. By contrasting the ABC reference table with a fake dataset under the same marginal distribution $\pi(X^{(n)})$, B-GAN learns to simulate from an approximation to the conditional distribution $\pi(\theta | X^{(n)})$. Similarly as Papamakarios and Murray (2016) and Lueckmann et al. (2017), our method is also global in the sense that it learns $\pi(\theta | X^{(n)})$ for *any* $X^{(n)}$, not necessarily $X_0^{(n)}$. More perfected posterior reconstructions can be obtained with post-processing steps that zoom in onto the posterior distribution evaluated at $X_0^{(n)}$. We consider two such refinements based on: (1) reinforcement learning with importance sampling, and (2) adversarial variational Bayes. We describe each approach below.

Simple rejection ABC may require exceedingly many trials to obtain only a few accepted samples when the posterior $\pi(\theta | X_0^{(n)})$ is much narrower than the prior $\pi(\theta)$ (see e.g. Marjoram et al. (2003); Sisson et al. (2007); Beaumont et al. (2009)). This has motivated query-efficient ABC techniques which intelligently decide where to propose next (see Jarvenpaa et al. (2020); Hennig and Schuler (2012) for decision-theoretic reasoning or Järvenpää et al. (2019) and Gutmann and Corander (2016) for implementations based on Bayesian optimization and surrogate models). Alternatively, Lueckmann et al. (2017) learn a Bayesian mixture density network approximating the posterior over multiple rounds of adaptively chosen simulations and use more flexible proposal distributions (not necessarily the prior) with a built-in importance-reweighting scheme. A similar strategy was used in Papamakarios et al. (2019) who used a pilot run of mixture density networks to learn the proposal distribution for the next round. Although $X_0^{(n)}$ is *not* used in B-GAN training, it can be used in the proposal inside the ABC reference table. Similarly as in Papamakarios et al. (2019), we use $X_0^{(n)}$ to construct a flexible proposal (i.e. an empirical Bayes prior) and

convert the draws to posterior samples under the original prior by importance reweighting. This ‘reinforcement learning’ refinement substantially improves the reconstruction accuracy and can be justified by theory.

Our vanilla B-GAN sampler uses contrastive learning (Gutmann et al., 2018; Durkan et al., 2020) to estimate the conditional distribution $\pi(\theta | X^{(n)})$ for *any* $X^{(n)}$. Since $X_0^{(n)}$ is used only at the evaluation stage (not the training stage), we can custom-make the sampler to $X_0^{(n)}$ by using the B-GAN output (or the output after reinforcement learning) as an initialization for implicit variational Bayes optimization (Tran et al., 2017; Huszár, 2017). Implicit variational Bayes attempts to approximate the posterior using densities which are defined implicitly by a push-forward mapping. B-GAN also trains such a mapping but the generator will have never seen observed data. At later stages of B-GAN training, we can thereby modify the objective function for the generator so that it minimizes a lower bound to the marginal likelihood. Since the likelihood cannot be evaluated, we use contrastive learning inside the variational objective to compute the lower bound (Huszár, 2017; Tran et al., 2017). We consider the joint-contrastive form (Huszár, 2017; Durkan et al., 2020), where the classifier is still trained to learn the joint likelihood ratio using the ABC reference table (similarly as in B-GAN). However, the generator is now trained on $X_0^{(n)}$ by maximizing the evidence lower bound. This algorithm is related to the B-GAN simulator, but uses $X_0^{(n)}$ during the training stage.

Contrastive learning has been used inside Bayesian likelihood-free sampling algorithms before (see e.g. Wang et al. (2022); Gutmann et al. (2018); Kaji and Ročková (2022)). Both Wang et al. (2022) and Kaji and Ročková (2022) assume iid data with a large enough sample size n to be able to apply classification algorithms for each iteration of Metropolis Hastings and ABC, respectively. Our approach does not require iid data and works even with $n = 1$. We also do not require to run classification at each posterior simulation step.

We show highly competitive performance of our methods (relative to state-of-the-art likelihood-free Bayesian methods) on several simulated examples. While conceptually related methodology has occurred before (Papamakarios and Murray, 2016; Lueckmann et al.,

2017; Ramesh et al., 2022), theory supporting these likelihood-free Bayesian approaches has been lacking. We provide new frequentist-Bayesian theoretical results for the typical variational distance between the true and approximated posteriors. We analyze Wasserstein versions of both the B-GAN algorithm as well as adversarial variational Bayes. With properly tuned neural networks, we show that this distance goes to zero as $n \rightarrow \infty$ with large enough ABC reference tables.

The outline of our paper is as follows. Section 2 reviews conditional GANs and introduces the Bayesian GAN sampler together with the reinforcement adjustments. In Section 3, we describe another local enhancement strategy inspired by implicit variational Bayes. In Section 4, we investigate the theoretical guarantees of the B-GAN posteriors. The performance of our methods is illustrated on simulated datasets in Section 5. In Section 6, we conclude with a discussion.

2 Adversarial Bayes

Generative Adversarial Networks (GANs) (Goodfellow et al., 2016) are a game-theoretic construct in artificial intelligence designed to simulate from likelihoods over complex objects. GANs involve two machines playing a game against one another. A *Generator* aims to deceive a *Discriminator* by simulating fake samples that resemble observed data while, at the same time, the Discriminator learns to tell the fake and real data apart. This process iterates until the generated data are indistinguishable by the Discriminator and can be regarded as genuine likelihood samples. Below, we review several recent GAN innovations and propose an incarnation for simulation from a posterior as opposed to a likelihood.

2.1 Vanilla GANs

In its simplest form, GANs learn how to implicitly simulate from the likelihood $p_{\theta_0}^{(n)}(\cdot)$ using only its realizations $X_0^{(n)} \in \mathcal{X}$ where $X_0^{(n)} \sim p_{\theta_0}^{(n)}$ when θ_0 is unknown. Recall that draws from implicit distributions can be obtained by passing a random noise vector $Z \in \mathcal{Z} \subseteq \mathbb{R}^d$

through a non-stochastic push-forward mapping $g_{\beta}(\cdot) : \mathcal{Z} \rightarrow \mathcal{X}$. The original GANs formulation (Goodfellow et al., 2016) involves a Generator, specified by the mapping $g_{\beta}(\cdot)$, that attempts to generate samples similar to $X_0^{(n)}$ by filtering Z , i.e.

$$X^{(n)} = (X_1, \dots, X_n)' \text{ where } X_i = g_{\beta}(Z_i) \text{ with } Z_i \stackrel{\text{iid}}{\sim} \pi_Z(Z) \text{ so that } X^{(n)} \sim p_{\theta}^{(n)}.$$

The generative coefficients β are iteratively updated depending on the feedback received from the Discriminator. The Discriminator, specified by a mapping $d(\cdot) : \mathcal{X} \rightarrow (0, 1)$, gauges similarity between $X^{(n)}$ and $X_0^{(n)}$ with a discrepancy between their (empirical) distributions. Hereafter we use X to denote a generic dataset as $X \in \mathcal{X}$ for simplicity of notation. At a population level, a standard way of comparing two distributions, say $P_{\theta_0}^{(n)}$ and $P_{\theta}^{(n)}$, is with the symmetrical Jensen-Shannon divergence¹ which can be equivalently written as a solution to a particular optimization problem

$$\text{JS}(P_{\theta}^{(n)}, P_{\theta_0}^{(n)}) = \ln 2 + 0.5 \times \sup_{d: \mathcal{X} \rightarrow (0,1)} \left\{ E_{X \sim P_{\theta}^{(n)}} \ln [d(X)] + E_{X \sim P_{\theta_0}^{(n)}} \ln [1 - d(X)] \right\}. \quad (2)$$

The optimal Discriminator $d^*(\cdot)$, solving the optimization (2), is $d^*(X) = p_{\theta}^{(n)}(X) / [p_{\theta}^{(n)}(X) + p_{\theta_0}^{(n)}(X)]$ (Goodfellow et al., 2014, Proposition 1). The optimal Generator is then defined through the optimal value β^* which leaves the Discriminator maximally confused, i.e. $d^*(X) = 1/2$ and therefore $p_{\theta}^{(n)}(X) = p_{\theta_0}^{(n)}(X)$ uniformly over \mathcal{X} .

Despite the nice connection to likelihood ratios, original GANs (Goodfellow et al., 2014) may suffer from training difficulties when the discriminator becomes too proficient early on (Gulrajani et al., 2017; Arjovsky and Bottou, 2017). Alternative divergences have been implemented inside GANs that are less prone to these issues. For example, the Wasserstein distance (Arjovsky and Bottou, 2017) also admits a dual representation

$$d_W(P_{\theta}^{(n)}, P_{\theta_0}^{(n)}) = \sup_{f \in \mathcal{F}_W} \left| E_{X \sim P_{\theta}^{(n)}} f(X) - E_{X \sim P_{\theta_0}^{(n)}} f(X) \right| \quad (3)$$

where $\mathcal{F}_W = \{f : \|f\|_L \leq 1\}$ are functions with a Lipschitz semi-norm $\|f\|_L$ at most one. The function $f(\cdot)$ is often referred to as the *Critic*. In our implementations, we will concentrate on the Wasserstein version of GANs (Arjovsky et al., 2017).

¹defined as $\text{JS}(P_{\theta}^{(n)}, P_{\theta_0}^{(n)}) = \text{KL}(P_{\theta}^{(n)} | (P_{\theta}^{(n)} + P_{\theta_0}^{(n)})/2) + \text{KL}(P_{\theta_0}^{(n)} | (P_{\theta}^{(n)} + P_{\theta_0}^{(n)})/2)$

2.2 Conditional GANs

While originally intended for simulating from likelihoods underlying observed data, GANs can be extended to simulating from distributions *conditional on* observed data. Certain aspects of conditional GANs (cGANs) have been investigated earlier (Gauthier, 2014; Mirza and Osindero, 2014) in various contexts including causal inference (Athey et al., 2021) or non-parametric regression (Zhou et al., 2022). Our work situates conditional GANs firmly within the context of ABC and likelihood-free posterior simulation. Before we describe our development in Section 2.3, we first introduce the terminology of cGANs within a Bayesian context. We will intentionally denote with X the conditioning variables and focus on the conditional distribution $\pi(\theta | X)$ for the inferential parameter $\theta \in \Theta$ with a prior $\pi(\theta)$. Similarly as with vanilla GANs in Section 2.1, cGANs again involve two adversaries represented by two mappings.

Definition 1. (*Generator*) We define a deterministic generative model as a mapping $g : (\mathcal{Z} \times \mathcal{X}) \rightarrow \Theta$ that filters noise random variables $Z \in \mathcal{Z}$ to obtain samples from an implicit conditional density $\pi_g(\theta | X)$. This conditional model then defines an implicit joint model $\pi_g(X, \theta) = \pi_g(\theta | X)\pi(X)$, where $\pi(X) = \int_{\Theta} p_{\theta}^{(n)}(X)\pi(\theta)d\theta$ is the marginal likelihood.

Definition 2. (*Discriminator*) We define a deterministic discriminative model as a mapping $d : (\mathcal{X} \times \Theta) \rightarrow (0, 1)$ which predicts whether the data pair (X, θ) came from $\pi(X, \theta)$ (label 1) or from $\pi_g(X, \theta)$ (label 0).

The main distinguishing feature, compared to vanilla GANs, is that the conditioning random vector X enters *both* mappings. The task is to flexibly parametrize $g_{\beta}(\cdot)$, e.g. using neural networks as will be seen later, in order to approximate the joint density model $\pi(X, \theta)$ as closely as possible. Ideally, we would like to recover an (oracle) function $g^* : \mathcal{Z} \times \mathcal{X} \rightarrow \Theta$ such that the conditional distribution of $g^*(Z, X)$ given X is the same as $\pi(\theta | X)$. The existence of such an oracle g^* is encouraged by the noise-outsourcing lemma from probability theory (Kallenberg, 2002; Zhou et al., 2022) which we reiterate below using Gaussian Z .

Lemma 1. (*Zhou et al., 2022, Lemma 2.1*) Let (X, θ) be a random pair taking values in $\mathcal{X} \times \Theta$ with a joint distribution $\pi(X, \theta)$. Then, for any given $d_z \geq 1$, there exists a random vector $Z \sim \pi_Z = N(0, I_{d_z})$ and a Borel-measurable function $g^* : \mathbb{R}^d \times \mathcal{X} \rightarrow \Theta$ such that Z is independent of X and $(X, \theta) = (X, g^*(Z, X))$ almost surely.

Although it is not necessary for Θ and Z to be of the same dimension d , we choose $\pi_Z = N(0, I_d)$ to balance the expressiveness of the generator and the discriminator.

The premise of conditional GANs rests in the fact that matching two joint distributions, while fixing a marginal distribution, is equivalent to matching conditional distributions. This implies that $g^*(Z, X)$, given X , is indeed distributed according to $\pi(\theta | X)$. The question remains how to find the oracle mapping g^* in practice. Using the Jensen-Shannon divergence (2) for comparing the joint distributions $\pi(X, \theta)$ and $\pi_g(X, \theta)$, the oracle mapping g^* emerges at the equilibrium of a minimax game.

Lemma 2. Consider a minimax game $(g^*, d^*) = \arg \min_{g \in \mathcal{G}} \max_{d \in \mathcal{D}} D(g, d)$ prescribed by

$$D(g, d) = E_{(X, \theta) \sim \pi(X, \theta)} \log d(X, \theta) + E_{X \sim \pi(X), Z \sim \pi_Z} \log[1 - d(X, g(Z, X))]. \quad (4)$$

Assume that \mathcal{G} and \mathcal{D} are universal approximators capable of representing any function $g : (\mathcal{Z} \times \mathcal{X}) \rightarrow \Theta$ and $d : (\mathcal{X} \times \Theta) \rightarrow (0, 1)$, respectively. Then, uniformly on \mathcal{X} and Θ , the solution (g^*, d^*) satisfies

$$\pi_{g^*}(\theta | X) = \frac{\pi(X, \theta)}{\pi(X)} = \pi(\theta | X) \quad \text{and} \quad d_g^*(X, \theta) = \frac{\pi(X, \theta)}{\pi(X, \theta) + \pi_g(X, \theta)} \quad \text{for any } g \in \mathcal{G}.$$

Proof. The expression for $d_g^*(X, \theta)$ is an immediate consequence of Proposition 1 in Goodfellow et al. (2014). Plugging-in this expression into (4), we find that

$$g^* = \arg \min_{g \in \mathcal{G}} \left(E_{(X, \theta) \sim \pi(X, \theta)} \log d_g^*(X, \theta) + E_{X \sim \pi(X), z \sim \pi_Z} \log[1 - d_g^*(X, g(Z, X))] \right),$$

According to Theorem 1 of Goodfellow et al. (2014), the minimum is achieved if and only if $\pi_{g^*}(X, \theta) = \pi(X, \theta) = \pi(\theta | X)\pi(X)$. The fact that $\pi(X, \theta)$ and $\pi_{g^*}(X, \theta)$ have the same marginal $\pi(X)$ implies the expression for $\pi_{g^*}(\theta | X)$. \square

While the Jensen-Shannon (JS) variant of the cGAN game in Lemma 2 is conceptually compelling and can be supported by theory (Zhou et al., 2022), implementation difficulties may arise (such as convergence failure or mode collapse (Arjovsky and Bottou, 2017)). We thereby focus on the Wasserstein variant of the game from Lemma 2

$$(g^*, f^*) = \arg \min_{g \in \mathcal{G}} \max_{f \in \mathcal{F}} \left| E_{X \sim \pi(X), Z \sim \pi_Z} f(X, g(Z, X)) - E_{(\theta, X) \sim \pi(X, \theta)} f(X, \theta) \right|, \quad (5)$$

where, using $\mathcal{F} = \mathcal{F}_W$, g^* minimizes the Wasserstein distance between $\pi_{g^*}(X, \theta)$ and $\pi(X, \theta)$. When \mathcal{G} and \mathcal{F} are expressive enough, the solution g^* also satisfies $\pi_{g^*}(\theta | X) = \pi(\theta | X)$.

2.3 Bayesian GANs

We now subsume the conditional GAN framework within the context of Bayesian simulation. To implement the adversarial game (5) in practice, one needs to (a) parametrize \mathcal{F} and \mathcal{G} (for instance using neural networks) and (b) to replace the expectations in (5) with empirical counterparts. Both of these steps will introduce approximation error. We provide theoretical insights later in Section 4.

We assume that the generator class $\mathcal{G} = \{g_\beta : (\mathcal{Z} \times \mathcal{X}) \rightarrow \Theta \text{ where } \beta \in \mathbb{R}^G\}$ is parametrized with β and the critic class $\mathcal{F} = \{f_\omega : (\mathcal{X} \times \Theta) \rightarrow \mathbb{R} \text{ where } \omega \in \mathbb{R}^C\}$ is parametrized with ω . We consider neural networks (with ReLU activations) in our implementations and support this choice with theory (Corollary 3).

For the empirical version, one can use the ABC reference table which consists of simulated data pairs $\{(\theta_j, X_j^{(n)})\}_{j=1}^T$ generated from the joint model $\pi(X^{(n)}, \theta) = p_\theta^{(n)}(X^{(n)})\pi(\theta)$ under the prior $\pi(\theta)$. We can think of each draw $X_j^{(n)} = (X_1^j, \dots, X_n^j)' \sim p_\theta^{(n)}$ as either a stacked collection of n iid q -dimensional variables X_i^j sampled from a product likelihood $\prod_{i=1}^n p_\theta(X_i^j)$ or a single observation from a general likelihood $p_\theta^{(n)}(\cdot)$ which may not necessarily assume independence (e.g. one time series observation vector). From now on, we will simply denote $X_j^{(n)}$ with X_j , similarly for $X_0^{(n)}$ and $X^{(n)}$.

We can break the relationship between θ and X in the ABC reference table by contrasting these data pairs with another dataset consisting of $\{(g(Z_j, X_j), X_j)\}_{j=1}^T$ where Z_j 's have

Algorithm 1 *B-GAN for Bayesian Simulation (Wasserstein Version).*

Input	
Prior $\pi(\theta)$, observed data X_0 and noise distribution $\pi_Z(\cdot)$	
Training	
Initialize network parameters $\omega^{(0)} = 0$ and $\beta^{(0)} = 0$	
Reference Table	
For $j = 1, \dots, T$:	Generate (X_j, θ_j) where $\theta_j \sim \pi(\theta)$ and $X_j \sim P_{\theta_j}^{(n)}$.
Wasserstein GAN	
For $t = 1, \dots, N$:	
Critic Update (N_{critic} steps): For $k = 1, \dots, N_{\text{critic}}$ Generate $Z_j \sim \pi_Z(z)$ for $j = 1, \dots, T$. Generate $\epsilon_j \stackrel{\text{iid}}{\sim} U[0, 1]$ and set $\bar{\theta}_j = \epsilon_j \theta_j + (1 - \epsilon_j) g_{\beta^{(t-1)}}(Z_j, X_j)$ for $j = 1, \dots, T$. Update $\omega^{(t)}$ by applying stochastic gradient descent on minimizing the objective function in (6) with the penalty (7).	
Generator Update (single step) Generate noise $Z_j \sim \pi_Z(z)$ for $j = 1, \dots, N$. Update $\beta^{(t)}$ by applying stochastic gradient descent on minimizing the objective function in (6).	
Posterior Simulation:	
For $i = 1, \dots, M$: Simulate $Z_i \sim \pi_Z(z)$ and set $\tilde{\theta}_i = g_{\beta^{(N)}}(Z_i, X_0)$.	

been sampled from $\pi_Z(\cdot)$. Keeping the same X_j 's essentially means that we are keeping the same marginal. The dataset $\{(g(Z_j, X_j), X_j)\}_{j=1}^T$ encapsulates iid draws from $\pi_g(X, \theta)$. These two datasets can be then used to approximate the expectations in (4) and (5). A high-level description of an algorithm for solving the Jensen-Shannon (JS) version of the game from Lemma 2 is outlined in Algorithm 4 (Appendix Section C). As mentioned earlier, the JS version may suffer from training issues (Arjovsky and Bottou, 2017). We provide an illustration of such issues using convergence diagnostics on a toy example in Section C.

In our implementations, we thereby consider the empirical version of (5) which again involves simulated datasets $\{(\theta_j, X_j)\}_{j=1}^T$ and $\{Z_j\}_{j=1}^T \stackrel{\text{iid}}{\sim} \pi_Z(\cdot)$ to obtain

$$\hat{\beta}_T = \arg \min_{\beta: g_{\beta} \in \mathcal{G}} \left[\max_{\omega: f_{\omega} \in \mathcal{F}_W} \left| \sum_{j=1}^T f_{\omega}(X_j, g_{\beta}(Z_j, X_j)) - \sum_{j=1}^T f_{\omega}(X_j, \theta_j) \right| \right]. \quad (6)$$

One particular way of solving this problem is summarized in Algorithm 1. In terms of the constraint on ω to ensure the Lipschitz condition $\|f_{\omega}\|_L \leq 1$, the original Wasserstein GANs implementation (Arjovsky and Bottou, 2017) used gradient clipping, which may lead to computational issues. Alternatively, Gulrajani et al. (2017) imposed a soft version of

the constraint with a penalty² on the gradient of f_ω with respect to a convex combination³ of the two contrasting datasets. Similarly as [Athey et al. \(2021\)](#), we adopt the one-sided penalty only with respect to θ_j

$$\lambda \left\{ \frac{1}{T} \sum_{j=1}^T \left[\max \left(0, \left\| \nabla_{\bar{\theta}_j} f_\omega(X_j, \bar{\theta}_j) \right\|_2 - 1 \right) \right]^2 \right\} \quad (7)$$

where $\bar{\theta}_j = \epsilon_j \theta_j + (1 - \epsilon_j) g(Z_j, X_j)$ with the ϵ_j re-drawn from a uniform distribution at each step. The choice of λ is discussed in [Appendix D](#). To stabilize gradients, the critic is updated multiple times (ideally until convergence) before each update of the generator, which is different from [Algorithm 4](#) where such a stabilization may not be feasible ([Arjovsky et al., 2017](#))

Our Bayesian GAN framework for posterior simulation (i.e. [Algorithm 1](#) further referred to as B-GAN) consists of a neural sampler $g_{\hat{\beta}_T}(Z, X)$ which generates samples from an approximate posterior, i.e. conditioning on the observed data X_0 , by filtering iid noise as follows

$$\tilde{\theta}_j = g_{\hat{\beta}_T}(Z_j, X_0) \quad \text{where} \quad Z_j \stackrel{\text{iid}}{\sim} \pi_Z(\cdot) \quad \text{for} \quad j = 1, \dots, M. \quad (8)$$

When $g_{\hat{\beta}_T}$ is close to g^* , the samples $\tilde{\theta}_j$ will arrive approximately from $\pi(\theta | X_0)$. One of the practical appeals of this sampling procedure is that, once the generator has been trained, the simulation cost is negligible. Note that our observed data $X_0 \sim p_{\theta_0}^{(n)}(X)$ are *not involved* in the training stage, *only* in the simulation stage [\(8\)](#). We illustrate [Algorithm 1](#) on a toy example. The configurations of our B-GAN networks and optimization hyperparameters are described in [Appendix D.1](#).

Example 1 (Toy Example). *This toy example (analyzed earlier in [Papamakarios et al. \(2019\)](#)) exposes the fragility of ABC methods in a relatively simple setting. The experiment entails $n = 4$ two-dimensional Gaussian observations $X = (x_1, x_2, x_3, x_4)'$ with $x_j \sim \mathcal{N}(\mu_\theta, \Sigma_\theta)$ parametrized by $\theta = (\theta_1, \theta_2, \theta_3, \theta_4, \theta_5)'$, where*

²They adopt the two-sided penalty encouraging the norm of the gradient to go towards 1 instead of just staying below 1 (one-sided penalty).

³This is inspired by the fact that the optimal critic function contains straight lines with gradient norm 1 connecting coupled points from the contrasted distributions ([Gulrajani et al., 2017](#), Proposition1).

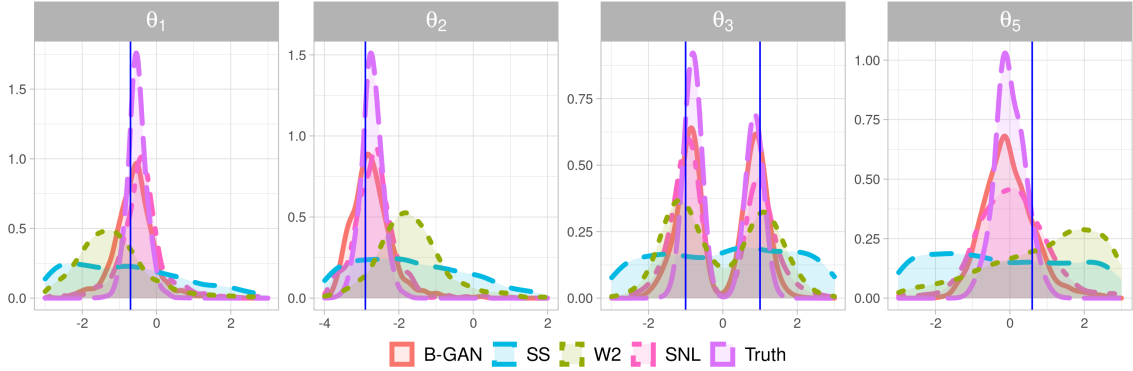


Figure 1: The approximated posteriors given by B-GAN, SNL, SS, and W2 for the toy example. The results for θ_4 are similar to θ_3 and thus not shown here.

$$\mu_{\theta} = (\theta_1, \theta_2)' \quad \text{and} \quad \Sigma_{\theta} = \begin{pmatrix} s_1^2 & \rho s_1 s_2 \\ \rho s_1 s_2 & s_2^2 \end{pmatrix}$$

with $s_1 = \theta_3^2, s_2 = \theta_4^2$ and $\rho = \tanh(\theta_5)$. The parameters θ are endowed with a uniform prior⁴. Approximating the posterior can be tricky because the signs of parameters θ_3 and θ_4 are not identifiable, yielding multimodality. We generate X_0 with parameters $\theta_0 = (-0.7, -2.9, -1.0, -0.9, 0.6)'$. Since we have access to the true posterior, we can directly compare our posterior reconstructions with the truth. We compare B-GAN with (1) ABC using naive summary statistics (SS) (mean and variance), (2) 2-Wasserstein distance ABC (Bernton et al., 2019), and (3) Sequential Neural Likelihood (SNL) (Papamakarios et al., 2019) with the default setting suggested by the authors. We provide all implementation details in Appendix D.1. For each method, we obtained $M = 1000$ samples and plotted them in Figure 1. Our B-GAN approach as well as SNL nicely capture the multimodality. There appears to be an overestimation of variance (relative to the truth) which, as we explain later in Section 4, is expected because B-GAN is trained to perform well on average for any X , not necessarily for X_0 . This motivates our two refinement strategies: one based on active learning (Section 2.4) and one based on variational Bayes (Section 3).

Similarly as with default ABC techniques, our B-GAN approach is not query-efficient, i.e. many prior guesses θ_j in the training dataset may be too far from the interesting areas

⁴on $[-3, 3] \times [-4, 4] \times [-3, 3] \times [-3, 3] \times [-3, 3]$

Algorithm 2 *2-Step Refinement (B-GAN 2step)*

INPUTPrior $\pi(\theta)$, observed data X_0 and noise distribution $\pi_Z(z)$ **Training**Initialize network parameters $\omega^{(0)} = 0$ and $\beta^{(0)} = 0$ **Pilot Run**Apply Algorithm 1 with $\pi(\theta)$ to learn $\hat{g}_{\text{pilot}}(\cdot)$ **Reference Table**Generate pairs $\{(X_j, \theta_j)\}_{j=1}^T$ where $\theta_j = \hat{g}_{\text{pilot}}(Z_j, X_0)$ for $Z_j \sim \pi_Z$ and $X_j \sim P_{\theta_j}^{(n)}$.**Refinement**Apply Wasserstein GAN step in Algorithm 1 on $\{(X_j, \theta_j)\}_{j=1}^T$ and return $g_{\hat{\beta}_T}(\cdot)$ **Posterior Simulation**Simulate $\{Z_i\}_{i=1}^M \stackrel{\text{iid}}{\sim} \pi_Z(z)$ and set $\tilde{\theta}_i = g_{\hat{\beta}_T}(Z_i, X_0)$.Estimate \hat{w}_i using either (9) or (10).**OUTPUT**Pairs of posterior samples and weights $(\tilde{\theta}_1, \hat{w}_1), \dots, (\tilde{\theta}_M, \hat{w}_M)$

with a likelihood support leaving only a few observations to learn about the conditional $\pi(\theta | X_0)$. The next section presents a two-step approach which uses X_0 for proposal construction in the ABC reference table to obtain more valuable data-points in the reference table.

2.4 Two-step Refinement

Our chief goal is to find a high-quality approximation to the conditional distribution $\pi(\theta | X)$ evaluated at the observed data $X = X_0$, not necessarily uniformly over the entire domain \mathcal{X} . However, the ABC reference table $\{(\theta_j, X_j)\}_{j=1}^T$ may not contain enough data points X_j in the vicinity of X_0 to train the simulator when the prior $\pi(\theta)$ is too vague. This can be remedied by generating a reference table using an auxiliary proposal distribution $\tilde{\pi}(\theta)$ which is more likely to produce pseudo-observations X_j that are closer to X_0 . For example, a pilot simulator $g_{\hat{\beta}_T}(Z, X_0)$ in (8) obtained from Algorithm 1 under the original prior $\pi(\theta)$ can be used to guide simulations in the next round to sharpen the reconstruction accuracy around

X_0 (Papamakarios and Murray, 2016). Training the generator⁵ $\tilde{g}_{\hat{\beta}_T}$ under the ‘wrong’ prior can be corrected for by importance re-weighting with weights $r(\theta) = \pi(\theta)/\tilde{\pi}(\theta)$. Since the posterior $\tilde{\pi}(\theta | X_0)r(\theta)$ is proportional to $\pi(\theta | X_0)$, reweighting the resulting samples $\tilde{\theta}_j = \tilde{g}_{\hat{\beta}_T}(Z, X_0^{(n)})$ with weights $w_j = r(\theta_j)$ will produce samples from an approximation to the original posterior (after normalization). Algorithm 2 summarizes this two-step strategy, referred to as B-GAN-2S.

Since the proposal density $\pi_{g_{\hat{\beta}_T}}(\theta | X_0)$ obtained in the pilot run *may not* have an analytical form, computing the importance weights $w_j = \pi(\theta_j)/\pi_{g_{\hat{\beta}_T}}(\theta_j | X_0)$ directly may not be feasible. We consider leaky ReLU generative networks for which, in fact, the analytical form does exist (Liang, 2021). More generally, the density ratio $r(\theta)$ can always be approximated. For example, with a tractable prior $\pi(\theta)$ the importance weights w_j can be estimated by

$$\hat{w}_j = \frac{\pi(\theta_j)}{\hat{\pi}_{g_{\hat{\beta}_T}}(\theta_j | X_0)} \quad (9)$$

where $\hat{\pi}_{g_{\hat{\beta}_T}}(\theta_j | X_0)$ is a plugged-in kernel density estimator (KDE) estimator (Terrell and Scott, 1992). This is particularly useful and efficient when the parameter dimension is low. When the prior is also not tractable but simulatable, the weights w_j can be directly estimated from classification by contrasting datasets $\tilde{\theta}_j \sim \tilde{\pi}(\theta)$ (label ‘0’) and $\theta_j \sim \pi(\theta)$ (label ‘1’). In particular, training a classifier \tilde{D} (see e.g. Cranmer et al. (2015); Durkan et al. (2020); Gutmann and Hyvärinen (2012) for the explanation of the ‘likelihood-ratio-trick’ for classification based estimators), we can obtain

$$\hat{w}_j = \frac{\tilde{D}(\tilde{\theta}_j)}{1 - \tilde{D}(\tilde{\theta}_j)}. \quad (10)$$

Papamakarios and Murray (2016) used mixture density networks estimators of the conditional distribution $\pi(\theta | x)$ after a pilot run to learn the proposal distribution $\tilde{\pi}(\theta)$. In order to obtain an analytically tractable Gaussian mixture representation, their proposal $\tilde{\pi}(\theta)$ has to be Gaussian and it cannot be narrower than any of the mixture components. We do not require such assumptions. Lueckmann et al. (2019) instead propose to directly

⁵which simulates from an approximation to $\tilde{\pi}(\theta | X_0) \propto p_{\theta_0}^{(n)}(X_0)\tilde{\pi}(\theta)$

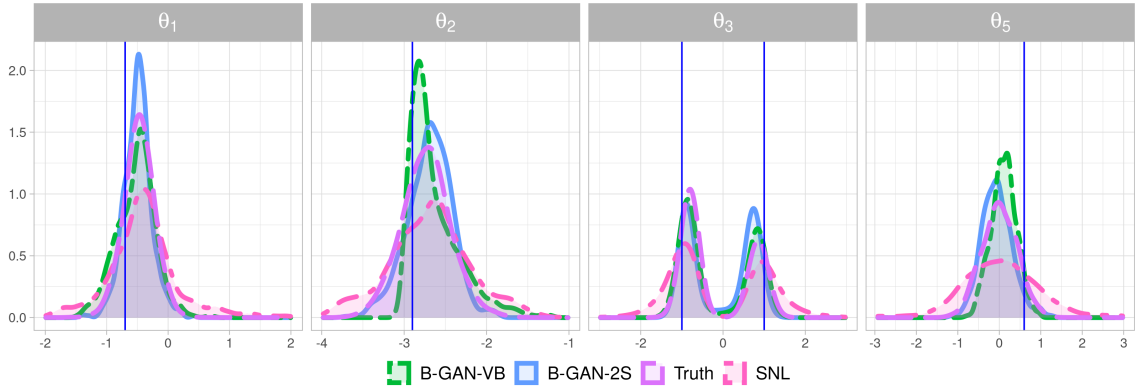


Figure 2: Posterior densities under the Gaussian model. The true parameter is $\theta_0 = (-0.7, -2.9, -1.0, -0.9, 0.6)'$, while the signs of θ_3 and θ_4 are not identifiable.

incorporate the weights $r(\theta)$ inside training and relax the Gaussianity assumption to avoid the variance instability. Similarly as in [Lueckmann et al. \(2019\)](#), we could also incorporate weights \hat{w}_j inside the objective function, e.g. multiplying each summand in (6) by \hat{w}_j .

Example 2 (Toy Example Continued). *We continue our exploration of the Toy Example 1. We now use the output from B-GAN (Algorithm 1) under the original uniform prior as a proposal distribution $\tilde{\pi}(\theta)$ and generate training data $\{(X_j, \theta_j)\}_{j=1}^T$ with a marginal $\tilde{\pi}(X) = \int_{\mathcal{X}} p_{\theta}^{(n)}(X) \tilde{\pi}(\theta) d\theta$. To revert the generated posterior samples to the original uniform prior, we perform reweighting by $r(\theta) = \pi(\theta) / \tilde{\pi}(\theta)$ using the kernel density estimator of $\tilde{\pi}(\theta)$ obtained from the pilot B-GAN run in Algorithm 1. The number of training points used in the second step is $T = 50\,000$. We note that much smaller T could be used if one were to perform more sequential refinements, not just one. The re-weighted (and normalized) posterior is plotted against the truth, SNL and a variational Bayesian variant (introduced later in Section 3) in Figure 2. Both B-GAN and B-GAN-2S provide tighter approximations to the true posterior. We repeated the experiment 10 times and report the Maximum Mean Discrepancies (MMD) ([Gretton et al., 2012](#)) between the true posterior and its approximations obtained from $M = 1\,000$ posterior draws for each method in Figure 3. Satisfyingly, B-GAN-2S yields the smallest MMD. We support this encouraging finding with our theoretical results in Section 4.*

Remark 1 (Computation When $n > 1$). *There are various ways of handling larger n . For*

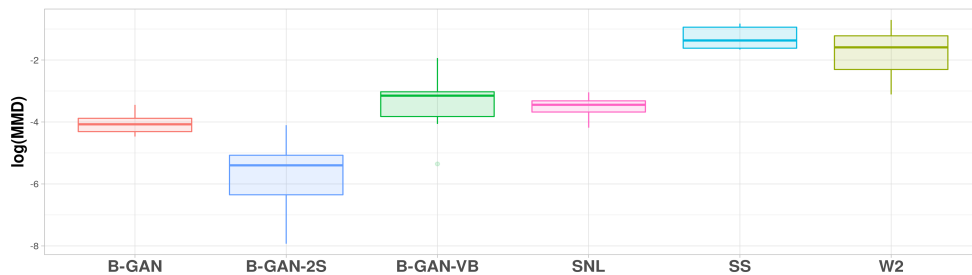


Figure 3: Maximum Mean Discrepancies (MMD, log scale) between the true posteriors and the approximated posteriors. The box-plots are computed from 10 repetitions.

example, our approach can be deployed sequentially on batches of smaller iid samplers: using simulations from a posterior on the smaller batch as a prior for the next. Alternatively, we could stack the n replicates into one data vector and learn a higher-dimensional mapping. Deep learning has been used for large sets of covariates and we regard this option doable when n and the dimensionality of the vectors is not overwhelmingly large.

In the two-step refinement, the observed data X_0 only contribute to the proposal distribution $\tilde{\pi}(\theta)$, not the training of the simulator $g_{\hat{\beta}}(\cdot)$. In the next section, we consider a variational Bayes variant which does involve X_0 in training.

3 Adversarial Variational Bayes

Variational Bayes (VB) is an optimization-centric Bayesian inferential framework based on minimizing a divergence between approximate and real posteriors. VB typically reduces the infinite-dimensional optimization problem to a finite-dimensional one by molding approximations into structured parametric forms. Implicit distributions (defined as probabilistic programs) have the potential to yield finer and tighter VB posterior approximations (Huszár, 2017; Kingma and Welling, 2013; Tran et al., 2017; Titsias and Ruiz, 2019). This section highlights the connection between the implicit variational Bayes inference and our B-GAN framework (Algorithm 1 and 2), both of which target the posterior.

The VB setup consists of an (intractable) likelihood $p_{\theta}^{(n)}(\cdot)$, prior $\pi(\theta)$ and a class of posterior approximations $q_{\beta}(\theta | X_0)$ indexed by β . We are recycling the notation of β here

to highlight the connection between the GAN generator and the the implicit variational generator. The goal of the VB approach is to find a set of parameters β^* that maximize a lower bound to the marginal likelihood

$$\log \pi(X_0) \geq \mathcal{L}(\beta) \equiv \int \log \left(\frac{\pi(X_0, \theta)}{q_\beta(\theta | X_0)} \right) q_\beta(\theta | X_0) d\theta. \quad (11)$$

The tightness of the inequality increases with expressiveness of the inference model $q_\beta(\cdot)$, where the equality occurs when $q_\beta(\theta | X_0) = \pi(\theta | X_0)$. Writing the evidence lower bound $\mathcal{L}(\beta) = -\text{KL}(q_\beta(\theta | X_0) || \pi(\theta | X_0)) + C$ in terms of Kullback-Leibler discrepancy, we have

$$\beta^* = \arg \max_{\beta} \mathcal{L}(\beta) = \arg \min_{\beta} \text{KL}(q_\beta(\theta | X_0) || \pi(\theta | X_0)). \quad (12)$$

Besides implicit likelihood, we also assume implicit posterior approximation $q_\beta(\theta | X)$. Similarly as before in Section 2.2, this approximation can be defined by stochastic generative networks which take a simple distribution and transform it nonlinearly by a deep neural network. In general, we assume that the density $q_\beta(\theta | X_0)$ *does not* have any particular form but, instead, that its samples are obtained by passing noise $Z \sim \pi_Z$ through a deterministic generator mapping $g_\beta(Z, X)$ parametrized by $\beta \in \mathbb{R}^G$.

With implicit likelihoods, where only forward simulation is possible, one may need to use contrastive learning (Bickel et al., 2007) to optimize the lower bound (11). Ideally, we would estimate the conditional density ratio by two contrasting datasets $\theta \sim \pi(\theta | X_0)$ (label ‘1’) and $\tilde{\theta} \sim q_\beta(\theta | X_0)$ (label ‘0’). However, this is not feasible since the posterior distribution $\pi(\theta | X_0)$ is unknown. Fortunately, we can simulate from (and contrast) two *joint* distributions with a different conditional, given X , but the same marginal $\pi(X)$. We define

$$\frac{d_{g_\beta}^*(X, \theta)}{1 - d_{g_\beta}^*(X, \theta)} = \frac{\pi(X, \theta)}{q_\beta(\theta | X)\pi(X)}, \quad (13)$$

where $d_{g_\beta}^* : (\mathcal{X} \times \Theta) \rightarrow (0, 1)$ can be viewed as the ‘oracle classifier’ when distinguishing data pairs (θ, X) as arising from either $\pi_{g_\beta}(\theta, X) \equiv q_\beta(\theta | X)\pi(X)$ or $\pi(\theta, X)$. We have seen this oracle classifier earlier in Lemma 2, with the variational conditional distribution $q_\beta(\theta | X)$ taking the place of $\pi_g(\theta | X)$. The variational lower bound (11) can be re-written

as

$$\mathcal{L}(\boldsymbol{\beta}) \equiv E_{\theta \sim q_{\boldsymbol{\beta}}(\theta | X_0)} \left[\text{logit} \left(d_{g_{\boldsymbol{\beta}}}^*(X_0, \theta) \right) \right] + C. \quad (14)$$

For implicit approximating distributions $q_{\boldsymbol{\beta}}(\theta | X)$ it may not be possible to directly optimize (14) with respect to $\boldsymbol{\beta}$ (even using the re-parametrization trick and stochastic gradient descent (Kingma and Welling, 2019)). The lower bound (14) depends on the oracle classifier which is unknown. Going back to Lemma 2, we note that $d_{g_{\boldsymbol{\beta}}}^*(\theta, X)$ is a solution to an infinite-dimensional classification problem under the entropy loss (Goodfellow et al., 2014)

$$d_{g_{\boldsymbol{\beta}}}^*(\theta, X) = \arg \max_{d \in \mathcal{D}} D(g_{\boldsymbol{\beta}}, d). \quad (15)$$

where $D(g_{\boldsymbol{\beta}}, d)$ was defined in (4) in Lemma 2. Although the oracle classifier is unknown, it can be estimated by solving a classification problem (15) by focusing on a particular class of classifiers $\mathcal{D} = \{d_{\phi} : (\mathcal{X} \times \Omega) \rightarrow (0, 1); \phi \in \mathbb{R}^C\}$, for instance neural networks indexed by parameters ϕ . We can thereby reframe maximizing the evidence lower bound (ELBO) in (14) as an adversarial game between two agents optimizing different objectives: (1) the *Generator* $g_{\boldsymbol{\beta}}(Z, X)$ tries to maximize ELBO, (2) the *Discriminator* $d_{\phi}(X, \theta)$ tries to distinguish between the two joint distributions. The idea of replacing aspects of the evidence lower bound with adversarial objectives occurred earlier (Mescheder et al., 2017; Huszár, 2017; Tran et al., 2017). These papers focus on hierarchical models with latent variables when either the prior or the likelihood (or both) are implicit. Instead of focusing on maximum likelihood estimation (Mescheder et al., 2017), we focus purely on VB inference with approximate posteriors $q_{\boldsymbol{\beta}}(\theta | X_0)$ when θ is assigned a prior.

All adversarial variational Bayesian papers have considered the KL formulation. Similarly as with the JS version of B-GAN (Algorithm 4), we have seen training issues (more discussion in Appendix B). We thereby resort to Wasserstein formulation (Ranganath et al., 2016; Ambrogioni et al., 2018) which minimizes the Wasserstein distance (instead of the KL divergence in (12))

$$\boldsymbol{\beta}^* = \arg \min_{\boldsymbol{\beta}: g_{\boldsymbol{\beta}} \in \mathcal{G}} \sup_{f_{\omega} \in \mathcal{F}_W} \left| E_{\theta \sim q_{\boldsymbol{\beta}}(\theta | X_0)} \left(\frac{\pi(\theta | X_0)}{q_{\boldsymbol{\beta}}(\theta | X_0)} - 1 \right) f_{\omega}(\theta) \right|, \quad (16)$$

where we have rewritten the Wasserstein distance (3) intentionally using density ratios and where the critic f_ω operates only on Θ . The parameters β^* can be approximated by replacing the density ratio with a classification estimator for the joint distributions (as discussed in Appendix B). We also implement a different algorithm which trains a critic on the joint space $\Theta \times \mathcal{X}$ without having to directly estimate the joint likelihood ratio.

Choosing \mathcal{F} that is symmetrical⁶, we start from $\beta^{(0)}$ and $\omega^{(0)}$ and using the reference table $\{(\theta_j, X_j)\}_{j=1}^T \stackrel{\text{iid}}{\sim} \pi(\theta, X)$ with $\{Z_j\}_{j=1}^T \stackrel{\text{iid}}{\sim} \pi_Z(\cdot)$, we

- update $\omega^{(t+1)}$ to approximate the Wasserstein distance, given $\beta^{(t)}$,

$$\omega^{(t+1)} = \arg \max_{\omega: f_\omega \in \mathcal{F}} \left[\sum_{j=1}^T f_\omega(X_j, g_{\beta^{(t)}}(Z_j, X_j)) - \sum_{j=1}^T f_\omega(X_j, \theta_j) \right] \quad (17)$$

- update $\beta^{(t+1)}$ to minimize the distance *evaluated at* X_0 , given $\omega^{(t+1)}$,

$$\beta^{(t+1)} = \arg \min_{\beta: g_\beta \in \mathcal{G}} \left[\sum_{j=1}^T f_{\omega^{(t+1)}}(X_0, g_\beta(Z_j, X_0)) + C \right], \quad (18)$$

where C does not depend on β , given the most recent update $\omega^{(t+1)}$. This iterative procedure can be regarded as targeting the estimator

$$\hat{\beta}_T = \arg \min_{\beta: g_\beta \in \mathcal{G}} \left| \frac{1}{T} \sum_{j=1}^T f_{\omega(\beta)}(X_0, g_\beta(Z_j, X_0)) - E_{\theta \sim \pi(\theta | X_0)} f_{\omega(\beta)}(X_0, \theta) \right| \quad (19)$$

where

$$\omega(\beta) = \arg \max_{\omega: f_\omega \in \mathcal{F}_W} \left| \frac{1}{T} \sum_{j=1}^T f_\omega(X_j, g_\beta(Z_j, X_j)) - \frac{1}{T} \sum_{j=1}^T f_\omega(X_j, \theta_j) \right|.$$

When we update $\beta^{(t+1)}$ given $\omega^{(t+1)}$, the second term in (19) does not depend on β and is consumed by the constant C in (18) in the iterative implementation. This iterative procedure resembles the GAN simulator (8). There are, however, fundamental differences compared to Algorithm 1. Unlike coefficients $\hat{\beta}_T$ in (6) of the B-GAN generator, coefficients $\hat{\beta}_T$ in (19) are *trained on* X_0 under the variational loss (14). This means that the generator $g_\beta(Z, X_0)$ directly targets $\pi(\theta | X)$ evaluated at $X = X_0$. We would thereby expect this version to work better than Algorithm 1 which does not use X_0 at all.

⁶i.e. $f_\omega \in \mathcal{F} \rightarrow -f_\omega \in \mathcal{F}$

Indeed, on the toy simulated example in Example 2 we can see that the VB variant produces tighter reconstructions relative to the B-GAN approach. The performance, however, is not uniformly better than Algorithm 2. We provide a snapshot from another repetition in Figure 6 (Appendix B.1), where the spikiness of B-GAN-VB (especially obvious when estimating θ_2) may explain why the MMDs between B-GAN-VB and the true posteriors are larger than for B-GAN-2S in Figure 3. The implementation details of B-GAN-VB are provided in Appendix B and the algorithm is described in Algorithm 3 (Section B.1). We initialize the generator at a network returned from Algorithm 2, see our discussion in Appendix B.3.

4 Theory

The purpose of this section is to provide theoretical solidification for the implicit posterior simulators in Algorithm 1, 2 and 3. We will quantify the typical total variation (TV) distance between the actual posterior and its approximation and illustrate that with carefully chosen neural generators and discriminators, the expected total variation distance vanishes as $n \rightarrow \infty$. We will continue denoting $X^{(n)}$ simply by X .

We define with $\nu = P_\theta^{(n)} \otimes \Pi$ the joint measure on $\mathcal{X} \times \Theta$ with a density $\pi(X, \theta) = p_\theta^{(n)}(X)\pi(\theta)$. The goal is to approximate this measure with μ_g defined semi-implicitly through a density function $\pi_g(X, \theta) = \pi(X)\pi_g(\theta | X)$ where $\pi(X) = \int \pi(X, \theta)d\theta$ is the marginal likelihood and where the samples from the density $\pi_g(\theta | X)$ are obtained by the *Generator* in Definition 1. Thus, by keeping the marginal distribution the same, the distribution $\pi_g(\theta | X)$ is ultimately approximating the conditional distribution $\pi(\theta | X)$. The quality of the approximation will be gauged under the integral probability metric⁷ (IPM)

$$d_{\mathcal{F}}(\mu_g, \nu) = \sup_{f \in \mathcal{F}} \left| E_{(X, \theta) \sim \mu_g} f(X, \theta) - E_{(X, \theta) \sim \nu} f(X, \theta) \right|, \quad (20)$$

where \mathcal{F} is a class of evaluation metrics⁸. The IPM metric (20), due to shared marginals

⁷The absolute value can be removed due to the Monge-Rubinstein dual (Villani, 2008).

⁸For example, Lipschitz-1 functions yield the Wasserstein-1 metric and functions bounded by 1 yield the TV metric.

of the two distributions, satisfies

$$d_{\mathcal{F}}(\mu_g, \nu) \leq E_X d_{\mathcal{F}}(\mu_g(X), \nu(X)), \quad (21)$$

where $\mu_g(X)$ and $\nu(X)$ denote the *conditional* measures with densities $\pi_g(\theta|X)$ and $\pi(\theta|X)$.

At the population level, the B-GAN (Algorithm 1) minimax game finds an equilibrium

$$g^* = \min_{g \in \mathcal{G}} d_{\mathcal{F}}(\mu_g, \nu),$$

where \mathcal{G} is a class of generating functions (that underlie the implicit distribution μ_g).

Typically, both \mathcal{F} and \mathcal{G} would be parameterized by neural networks with the hope that the discriminator networks can closely approximate the metric $d_{\mathcal{F}}$ and that the generator networks can flexibly represent distributions. In practice, one would obtain a data-driven estimator based on the *empirical* distribution $\bar{\nu}_T$ of (θ_j, X_j) for $1 \leq j \leq T$ and the *empirical* distribution $\bar{\mu}_g$ of $(g(Z_j, X_j), X_j)$ where $Z_j \sim \pi_Z$ for $1 \leq j \leq T$. Assuming that $\mathcal{G} = \{g_{\beta} : \beta \in \mathbb{R}^G\}$, the B-GAN estimator can be written as

$$\hat{\beta}_T \in \arg \min_{\beta: g_{\beta} \in \mathcal{G}} \max_{\omega: f_{\omega} \in \mathcal{F}} \left| E_{\bar{\mu}_g} f_{\omega}(X, g_{\beta}(Z, X)) - E_{\bar{\nu}_T} f_{\omega}(X, \theta) \right|. \quad (22)$$

For brevity, we will often denote the generator density $\pi_{g_{\beta}}(\cdot)$ (see Definition 1) simply by $\pi_{\beta}(\cdot)$ and similarly for $\mu_{g_{\beta}}$. The next Theorem provides an upper bound on the typical total variation (TV) distance between true and the approximated posterior measures $\nu(X_0)$ and $\mu_{\hat{\beta}_T}(X_0)$ with densities $\pi(\theta|X_0)$ and $\pi_{\hat{\beta}_T}(\theta|X_0)$, respectively. The total variation distance can be upper bounded by three terms: (1) the ability of the critic to tell the true model apart from the approximating model

$$\mathcal{A}_1(\mathcal{F}, \mathcal{G}) \equiv \mathbb{E} \inf_{\omega: f_{\omega} \in \mathcal{F}} \left\| \log \frac{\pi(\theta|X)}{\pi_{\hat{\beta}_T}(\theta|X)} - f_{\omega}(X, \theta) \right\|_{\infty} \quad (23)$$

(2) the ability of the generator to approximate the average true posterior

$$\mathcal{A}_2(\mathcal{G}) \equiv \inf_{\beta: g_{\beta} \in \mathcal{G}} \left[E_X \left\| \log \frac{\pi_{\beta}(\theta|X)}{\pi(\theta|X)} \right\|_{\infty} \right]^{1/2}, \quad (24)$$

and (3) the complexity of the (generating and) critic function classes measured the pseudo-dimension $Pdim(\cdot)$ and defined in Definition 2 in Bartlett et al. (2017). We denote with

$\mathcal{H} = \{h_{\omega, \beta} : h_{\omega, \beta}(Z, X) = f_{\omega}(g_{\beta}(Z, X), X)\}$ a structured composition of networks $f_{\omega} \in \mathcal{F}$ and $g_{\beta} \in \mathcal{G}$.

Theorem 1. Let $\hat{\beta}_T$ be as in (22) where $\mathcal{F} = \{f : \|f\|_{\infty} \leq B\}$ for some $B > 0$. Denote with \mathbb{E} the expectation with respect to empirical measure on $\{(X_j, \theta_j)\}_{j=1}^T$ and $\{Z_j\}_{j=1}^T$ in the reference table. Assume that the prior satisfies

$$\mathbb{P}[B_n(\theta_0; \epsilon)] \geq e^{-C_2 n \epsilon^2} \quad \text{for some } C_2 > 0 \text{ and } \epsilon > 0, \quad (25)$$

where the KL neighborhood $B_n(\theta_0; \epsilon)$ is defined as

$$B_n(\theta_0; \epsilon) = \{\theta \in \Theta : KL(P_{\theta_0}^{(n)} \| P_{\theta}^{(n)}) \leq n \epsilon^2, V_{2,0}(P_{\theta_0}^{(n)}, P_{\theta}^{(n)}) \leq n \epsilon^2\}. \quad (26)$$

Then for $T \geq Pdim(\mathcal{F}) \vee Pdim(\mathcal{H})$ we have for any $C > 0$

$$P_{\theta_0}^{(n)} \mathbb{E} d_{TV}^2(\nu(X_0), \mu_{\hat{\beta}_T}(X_0)) \leq C_n^T(\epsilon, C),$$

where, for some $\tilde{C} > 0$ and $Pmax \equiv Pdim(\mathcal{F}) \vee Pdim(\mathcal{H})$,

$$C_n^T(\epsilon, C) = \frac{1}{C^2 n \epsilon^2} + \frac{e^{(1+C_2+C)n\epsilon^2}}{4} \left[2\mathcal{A}_1(\mathcal{F}, \mathcal{G}) + \frac{B \mathcal{A}_2(\mathcal{G})}{\sqrt{2}} + 4\tilde{C} B \sqrt{\frac{\log T \times Pmax}{T}} \right].$$

Proof. Section A.1

From (21), it can be seen that Algorithm 1 targets a lower bound to the average Wasserstein distance between the posterior $\pi(\theta | X)$ and $\pi_g(\theta | X)$ after marginalizing over $\pi(X)$. In other words, Algorithm 1 is not necessarily targeting $\pi(\theta | X_0)$. The 2-step enhancement in Algorithm 2 provides more data draws in the ABC table that more closely resemble X_0 . Theorem 1 applies to Algorithm 2 as well with slight modifications.

Corollary 1. (2step B-GAN) Assume that $\hat{\beta}_T$ in (22) is learned under the proposal distribution $\tilde{\pi}(\theta)$ and denote with $\tilde{\mathbb{E}}$ the expectation of the reference table under $\tilde{\pi}(\theta)$. Assume that the original prior $\pi(\theta)$ satisfies (25). Then the importance re-weighted posterior reconstruction from Algorithm 2 satisfies the statement in Theorem 1 with \mathbb{E} replaced by $\tilde{\mathbb{E}}$ and with $\tilde{\mathcal{A}}_2(\mathcal{G}) \equiv \inf_{\beta: g_{\beta} \in \mathcal{G}} \left[\int_{\mathcal{X}} \tilde{\pi}(X) \left\| \log \frac{\pi_{\beta}(\theta | X)}{\pi(\theta | X)} \right\|_{\infty} dX \right]^{1/2}$ and $\tilde{\mathcal{A}}_1(\mathcal{F}, \mathcal{G}) \equiv \tilde{\mathbb{E}} \inf_{\omega: f_{\omega} \in \mathcal{F}} \left\| \frac{\pi(\theta)}{\pi(\theta)} \log \frac{\pi(\theta | X)}{\pi_{\hat{\beta}_T}(\theta | X)} - f_{\omega}(X, \theta) \right\|_{\infty}$.

Proof. Section [A.2](#)

Remark 2. *Zhou et al. (2022) provided theoretical results for the total variation distance between joint distributions using the Jensen-Shannon version of conditional GANs. Contrastingly, we provide frequentist-Bayesian results, quantifying the typical total variation distance between the true and approximate posteriors. In addition, we use the Wasserstein GANs, building on oracle inequalities established in Liang (2021).*

The (nonasymptotic) bounds for the *typical* TV distance in Theorem [1](#) and Corollary [1](#) are not refined enough to fully appreciate the benefits of the 2-step enhancement. In Remark [4](#) in Appendix (Section [A.3](#)), we provide an intuitive explanation for why the 2-step refinement version works so well in practice on each particular realization of X_0 (not only on average over many realizations X_0). We also provide a version of Theorem [1](#) for adversarial variational Bayes (Algorithm [3](#)) in Theorem [2](#) (Section [A.5](#)).

One of the appeals of our method is that it can accommodate situations where $n = 1$ (such as spatiotemporal dependent datasets). For n independent copies of observed data vectors, it is desirable to inquire when the average total variation distance in Theorem [1](#) converges to zero as $n \rightarrow \infty$ for a suitable choice of ϵ and C (potentially depending on n). We provide one example using discriminator feed-forward networks \mathcal{F} with a ReLU activation function $\sigma_{ReLU}(x) = \max\{x, 0\}$ which have good approximation properties (Schmidt-Hieber, 2020). For the generator networks, we need to make sure that the resulting density $\pi_g(\theta | X)$ is absolutely continuous. To this end, we consider \mathcal{G} that are leaky feed-forward ReLU neural networks with an activation function $\sigma_{ReLU}^a(x) = \max\{ax, x\}$ for some $0 < a \leq 1$. Liang (2021, Section 3.3) shows that these networks indeed produce densities that are absolutely continuous and provided a closed-form expression for the log density.

Definition 3. *We denote with $\mathcal{F}_L^B(S, W)$ a class of feed-forward ReLU neural networks f with depth L (i.e. the number of hidden layers plus one), width W and size S (total number of parameters in the network) such that $\|f\|_\infty \leq B$. The width is defined as $W = \max\{w_0, \dots, w_L\}$ where w_l is the width of the l^{th} layer with w_0 the input data dimension*

and w_L the output dimension. With $\mathcal{G}_L^B(S, W)$, we denote the leaky ReLU neural networks with the same meaning of parameters.

The following remark (clarified in Section A.4 in the Appendix) warrants optimism when using neural networks for the generator and the discriminator. We formulate the remark for Algorithm 1 and note that a similar conclusion holds for Algorithm 2 as well.

Remark 3. Assume that the joint distribution $\pi(\theta, X)$ is realizable in the sense that there exists $g_{\beta_0} \in \mathcal{G}_{L_0}^{B_0}(S_0, W_0)$ such that $\pi(\theta, X) = \pi_{g_{\beta_0}}(\theta, X)$. Assume that $\mathcal{G}_{L^*}^{B^*}(S^*, W^*) \subseteq \mathcal{G}_{L_0}^{B_0}(S_0, W_0)$ is a class of leaky ReLU generative networks indexed by β where $\|\beta_0\|_\infty \vee \|\beta\|_\infty \leq b$ for some $b > 0$. Assume that $\mathcal{F} = \mathcal{F}_L^B(S, W)$ are ReLU discriminator networks and π_Z is uniform on $[0, 1]^d$. Assume the prior concentration (25) is satisfied with $\epsilon_n > 0$ such that $\epsilon_n = O(1/\sqrt{n})$. For each arbitrarily slowly increasing sequence C_n , there exists $L, S, W > 0$ and T_n such that we have $P_{\theta_0}^{(n)} \mathbb{E} d_{TV}^2(\nu(X_0), \mu_{\hat{\beta}_{T_n}}(X_0)) = o(1)$ as $n \rightarrow \infty$.

5 Performance Evaluation

This section demonstrates very promising performance of our B-GAN approaches in Algorithm 1 (B-GAN), Algorithm 2 (B-GAN-2S) and Algorithm 3 (B-GAN-VB) and on simulated examples relative to other Bayesian likelihood-free methods (plain ABC using summary statistics (SS); 2-Wasserstein distance ABC by [Bernton et al. \(2019\)](#); Sequential Neural Likelihood (SNL) ([Papamakarios et al., 2019](#)) with default settings). The implementation details of our methods and the counterparts are described in Appendix D.2 for the Lotka-Volterra model and Appendix D.3 for the Boom-and-Bust model.

5.1 Lotka-Volterra Model

The Lotka-Volterra (LV) predator-prey model ([Wilkinson, 2018](#)) is one of the classical likelihood-free examples and describes population evolutions in ecosystems where predators interact with prey. The state of the population is prescribed deterministically via a system of ordinary differential equations (ODEs). Inference for such models is challenging because

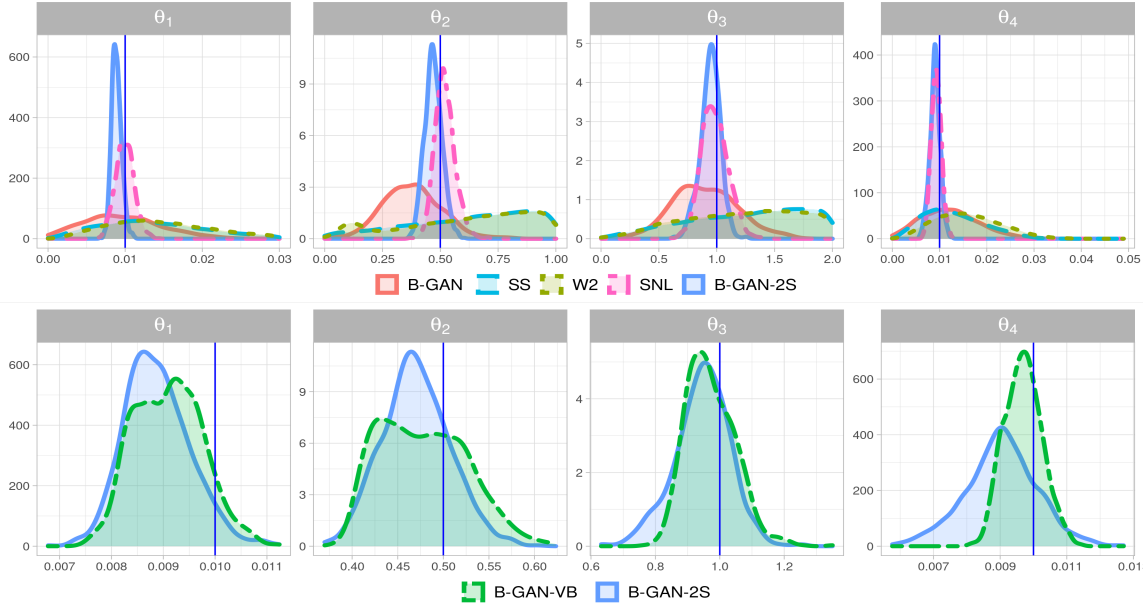


Figure 4: Approximate posterior densities under the Lotka-Volterra Model. The true parameter vector (marked by vertical lines) is $\theta_0 = (0.01, 0.5, 1, 0.01)'$.

the transition density is intractable. However, simulation from the model is possible, which makes it a natural candidate for simulator-based inference methods.

The model monitors population sizes of predators x_t and prey y_t over time t . The changes in states are determined by four parameters $\theta = (\theta_1, \dots, \theta_4)'$ controlling: (1) the rate $r_1^t = \theta_1 x_t y_t$ of a predator being born; (2) the rate $r_2^t = \theta_2 x_t$ of a predator dying; (3) the rate $r_3^t = \theta_3 y_t$ of a prey being born; (4) the rate $r_4^t = \theta_4 x_t y_t$ of a prey dying. Given the initial population sizes (x_0, y_0) at time $t = 0$, the dynamics can be simulated using the Gillespie algorithm (Gillespie, 1977), which is a stochastic discrete-time Markov chain model. The algorithm samples times to an event from an exponential distribution (with a rate $\sum_{j=1}^4 r_j^t$) and picks one of the four reactions with probabilities proportional to their individual rates r_j^t . We use the same setup as Kaji and Ročková (2022) where each simulation is started at $x_0 = 50$ and $y_0 = 100$ and state observations are recorded every 0.1 time units for a period of 20 time units, resulting in a series of 201 observations each.

The real data X_0 are generated with true values $\theta_0 = (0.01, 0.5, 1, 0.01)'$. The data vector X_0 is stretched into one $(201 \times 2 \times n)$ vector. The advantage of our approach is

that it can be used even for $n = 1$ when other methods (such as [Kaji and Ročková \(2022\)](#)) cannot. We focus on the $n = 1$ case here. We use an informative prior $\theta \in U(\Xi)$ with a restricted domain $\Xi = [0, 0.1] \times [0, 1] \times [0, 2] \times [0, 0.1]$ to make it easier for classical ABC methods (see [Kaji and Ročková \(2022\)](#)) and to make the GAN training more efficient. Previous analyses ([Papamakarios and Murray, 2016](#)) suggested summary statistics as the mean, log-variance, autocorrelation (at lag 1 and 2) of each series as well as their correlation. [Papamakarios et al. \(2019\)](#) also built their sequential neural network on top of this set of summary statistics. We build our model on the time series itself. This example is quite challenging due to the spikiness of the likelihood in very narrow areas of the parameter space (as explained in [Kaji and Ročková \(2022\)](#)). Our adversarial approaches are implemented using the Wasserstein versions.

To recover the posterior distributions, we draw $M = 1000$ samples for each method, except the top 1% for the ABC methods. A typical snapshot (for one particular data realization) of the approximated posteriors is given in [Figure 4](#) and the summary statistics averaged over 10 repetitions are reported in [Table 1](#). Since we do not have access to the true posterior, we look at the width of the 95% credible interval, its coverage (proportion of the 10 replications such that the true value is inside the credible interval), and bias of the posterior mean. Again, we observe that B-GAN-2S and B-GAN-VB outperforms B-GAN and SNL with a smaller bias and tighter variance. In [Figure 4](#), B-GAN-VB appears to have smaller bias than B-GAN-2S when estimating all parameters but θ_1 . The computation cost requirements are compared in [Section D.5](#).

5.2 Simple Recruitment, Boom and Bust

Our second demonstration is on the simple recruitment, boom and bust model ([Fasiolo et al., 2018](#)). The model is prescribed by a discrete stochastic process, characterizing the fluctuation of the population size of a certain group over time. Given the population size N_t and parameter $\theta = (r, \kappa, \alpha, \beta)'$, the population size at the next timestep N_{t+1} follows

(scale)	$\theta_1 = 0.01$		$\theta_2 = 0.5$		$\theta_3 = 1.0$		$\theta_4 = 0.01$	
	bias	CI width	bias	CI width	bias	CI width	bias	CI width
	($\times 10^{-3}$)	($\times 10^{-2}$)	($\times 10^{-1}$)				($\times 10^{-2}$)	($\times 10^{-2}$)
B-GAN	4.15	1.89	1.09	0.45	0.24	1.00	0.49	2.18
B-GAN-2S	0.70	0.21 (0.9)	0.42	0.10 (0.7)	0.11	0.33 (0.9)	0.13	0.34 (0.8)
B-GAN-VB	1.02	0.25 (0.7)	0.38	0.11 (0.9)	0.11	0.29 (0.8)	0.12	0.29 (0.7)
SNL	1.05	0.44	0.45	0.17	0.13	0.48	0.15	0.52
SS	9.58	3.80	2.49	0.91	0.49	1.76	0.68	2.72
W2	10.99	4.02 (0.9)	2.42	0.84	0.47	1.73	0.79	2.82

Table 1: Summary statistics of the approximated posteriors under the Lotka-Volterra model (averaged over 10 repetitions). Bold fonts mark the best model of each column. The coverage of the 95% credible intervals are 1 unless otherwise noted in the parentheses.

the following distribution

$$N_{t+1} \sim \begin{cases} \text{Poisson}(N_t(1+r)) + \epsilon_t, & \text{if } N_t \leq \kappa \\ \text{Binom}(N_t, \alpha) + \epsilon_t, & \text{if } N_t > \kappa \end{cases},$$

where $\epsilon_t \sim \text{Pois}(\beta)$ is a stochastic arrival process, with rate $\beta > 0$. The population grows stochastically at rate $r > 0$, but it crashes if the carrying capacity κ is exceeded. The survival probability $\alpha \in (0, 1)$ determines the severity of the crash. Over time the population fluctuates between high and low population sizes for several cycles.

This model has been shown to be extra challenging for both synthetic likelihood (SL) methods and ABC methods in [Fasiolo et al. \(2018\)](#). The distribution of the statistics is far from normal which breaks the normality assumption of SL. In addition, the authors show that ABC methods require exceedingly low tolerances and low acceptance rates to achieve satisfying accuracy.

We first run the simulation study using the setup in [An et al. \(2020\)](#). The real data X_0 is generated using parameters $r = 0.4, \kappa = 50, \alpha = 0.09$ and $\beta = 0.05$, and the prior distribution is uniform on $[0, 1] \times [10, 80] \times [0, 1] \times [0, 1]$. The observed data has 250 time-steps, with 50 burn-in steps to remove the transient phase of the process.

Previous analyses of the model suggested various summary statistics, including the mean, variance, skewness, kurtosis of the data, lag 1 differences, and lag 1 ratios ([An et al.](#),

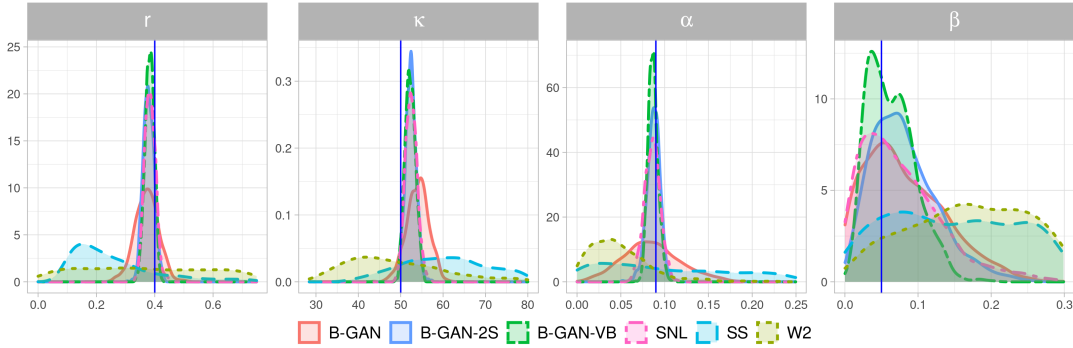


Figure 5: Approximate posterior densities under the Boom-and-Bust Model. The true parameter is $\theta_0 = (0.01, 0.5, 1, 0.01)'$.

2020). We use them in SS and SNL methods. We have explored three types of input: the time series itself, the time series in conjunction with their summary statistics, and the summary statistics only. We find that the network built on the summary statistics appears to perform the best, thus we only include the results from this network here.

We include SS, W2, SNL as competitors for comparisons. One snapshot of the approximate posterior densities is provided in Figure 5. We report the performance summary averaged over 10 repetitions in Table 2. ABC methods struggle to identify the parameters and provide very flat posteriors. The vanilla B-GAN is able to identify the correct location of parameters but with rather wide credible intervals. We observe great improvements after applying the 2-step refinements, the most obvious one for the parameter α . SNL, B-GAN-2S and B-GAN-VB are all able to provide very accurate estimates with tight credible intervals. B-GAN-VB provides the smallest bias and the tightest posteriors, especially for β , although at the cost of lower coverage. While B-GAN-VB is performing better, the performance of B-GAN-2S is slightly inferior relative to SNL in this example. Potentially, the performance of B-GAN-2S can be further improved if we add more sequential refinement steps in B-GAN-2S training, since the prior range here is too wide.

(scale)	$r = 0.4$		$\kappa = 50$		$\alpha = 0.09$		$\beta = 0.05$	
	bias	CI width	bias	CI width	bias	CI width	bias	CI width
	($\times 10^{-1}$)	($\times 10^{-1}$)			($\times 10^{-2}$)	($\times 10^{-1}$)	($\times 10^{-1}$)	
B-GAN	0.44	1.63	2.92	10.78	3.03	1.38	1.22	0.36 (0.8)
B-GAN-2S	0.27	0.79 (0.8)	1.60	5.29 (0.9)	1.06	0.34	1.05	0.26 (0.7)
B-GAN-VB	0.23	0.65 (0.8)	1.29	4.88 (0.9)	0.89	0.25 (0.7)	1.00	0.19 (0.5)
SNL	0.24	0.93	1.52	5.37	1.01	0.38	1.28	0.39 (0.9)
SS	2.16	8.26	10.60	37.17	15.08	9.18	4.41	0.95
W2	2.59	9.49	10.16	43.20	5.46	2.77	3.92	0.86 (0.6)

Table 2: Summary statistics of the approximated posteriors under the Boom-and-Bust model (averaged over 10 repetitions). Bold fonts mark the best model of each column. The coverage of the 95% credible intervals are 1 unless otherwise noted in the parentheses.

6 Discussion

This paper proposes strategies for Bayesian simulation using generative networks. We have formalized several schemes for implicit posterior simulation using GAN conditional density regression estimators as well as implicit variational Bayes. The common denominator behind our techniques is (joint) contrastive adversarial learning (Tran et al., 2017; Huszár, 2017). We have provided firm theoretical support in the form of bounds for the typical total variation distance between the posterior and its approximation. We have highlighted the potential of our adversarial samplers on several simulated examples with very encouraging findings. We hope that our paper will embolden practitioners to implement neural network posterior samplers in difficult situations when likelihood (and prior) are implicit.

Acknowledgments

The authors gratefully acknowledge support from the James S. Kemper Research Fund at the Booth School of Business and the National Science Foundation (DMS: 1944740).

References

- Ambrogioni, L., Güçlü, U., Güçlütürk, Y., Hinne, M., van Gerven, M. A., and Maris, E. (2018). Wasserstein variational inference. *Advances in Neural Information Processing Systems*, 31.
- An, Z., Nott, D. J., and Drovandi, C. (2020). Robust Bayesian synthetic likelihood via a semi-parametric approach. *Statistics and Computing*, 30(3):543–557.
- Anthony, M. and Bartlett, P. L. (1999). *Neural network learning: Theoretical foundations*, volume 9. Cambridge University Press.
- Arjovsky, M. and Bottou, L. (2017). Towards principled methods for training generative adversarial networks. In *International Conference on Learning Representations*.
- Arjovsky, M., Chintala, S., and Bottou, L. (2017). Wasserstein generative adversarial networks. In *International Conference on Machine Learning*, pages 214–223. PMLR.
- Athey, S., Imbens, G. W., Metzger, J., and Munro, E. (2021). Using Wasserstein generative adversarial networks for the design of Monte Carlo simulations. *Journal of Econometrics*.
- Bartlett, P. L., Foster, D. J., and Telgarsky, M. J. (2017). Spectrally-normalized margin bounds for neural networks. *Advances in Neural Information Processing systems*, 30.
- Beaumont, M. A. (2003). Estimation of population growth or decline in genetically monitored populations. *Genetics*, 164(3):1139–1160.
- Beaumont, M. A., Cornuet, J.-M., Marin, J.-M., and Robert, C. P. (2009). Adaptive approximate Bayesian computation. *Biometrika*, 96(4):983–990.
- Beaumont, M. A., Zhang, W., and Balding, D. J. (2002). Approximate Bayesian computation in population genetics. *Genetics*, 162(4):2025–2035.

- Bernton, E., Jacob, P. E., Gerber, M., and Robert, C. P. (2019). Approximate Bayesian computation with the Wasserstein distance. *Journal of the Royal Statistical Society: Series B (Statistical Methodology)*, 81(2):235–269.
- Bickel, S., Brückner, M., and Scheffer, T. (2007). Discriminative learning for differing training and test distributions. In *Proceedings of the 24th International Conference on Machine Learning*, pages 81–88.
- Blum, M. G. and François, O. (2010). Non-linear regression models for approximate Bayesian computation. *Statistics and Computing*, 20(1):63–73.
- Burkard, R., Dell’Amico, M., and Martello, S. (2009). *Assignment problems*. SIAM.
- Chen, X. and White, H. (1999). Improved rates and asymptotic normality for nonparametric neural network estimators. *IEEE Transactions on Information Theory*, 45(2):682–691.
- Cranmer, K., Pavez, J., and Louppe, G. (2015). Approximating likelihood ratios with calibrated discriminative classifiers. *arXiv preprint arXiv:1506.02169*.
- Cuturi, M. (2013). Sinkhorn distances: Lightspeed computation of optimal transport. *Advances in Neural Information Processing Systems*, 26.
- Durkan, C., Murray, I., and Papamakarios, G. (2020). On contrastive learning for likelihood-free inference. In *International Conference on Machine Learning*, pages 2771–2781. PMLR.
- Fasiolo, M., Wood, S. N., Hartig, F., and Bravington, M. V. (2018). An extended empirical saddlepoint approximation for intractable likelihoods. *Electronic Journal of Statistics*, 12(1):1544–1578.
- Frazier, D. T., Martin, G. M., Robert, C. P., and Rousseau, J. (2018). Asymptotic properties of approximate Bayesian computation. *Biometrika*, 105(3):593–607.

- Gauthier, J. (2014). Conditional generative adversarial nets for convolutional face generation. *Class project for Stanford CS231N: convolutional neural networks for visual recognition, Winter semester, 2014(5):2*.
- Ghosal, S. and Van Der Vaart, A. (2007). Convergence rates of posterior distributions for noniid observations. *The Annals of Statistics*, 35(1):192–223.
- Gillespie, D. T. (1977). Exact stochastic simulation of coupled chemical reactions. *The Journal of Physical Chemistry*, 81(25):2340–2361.
- Goodfellow, I., Bengio, Y., and Courville, A. (2016). *Deep learning*. MIT press.
- Goodfellow, I., Pouget-Abadie, J., Mirza, M., Xu, B., Warde-Farley, D., Ozair, S., Courville, A., and Bengio, Y. (2014). Generative adversarial nets. *Advances in Neural Information Processing Systems*, 27.
- Gretton, A., Borgwardt, K. M., Rasch, M. J., Schölkopf, B., and Smola, A. (2012). A kernel two-sample test. *The Journal of Machine Learning Research*, 13(1):723–773.
- Gulrajani, I., Ahmed, F., Arjovsky, M., Dumoulin, V., and Courville, A. C. (2017). Improved training of Wasserstein gans. *Advances in Neural Information Processing Systems*, 30.
- Gutmann, M. U. and Corander, J. (2016). Bayesian optimization for likelihood-free inference of simulator-based statistical models. *Journal of Machine Learning Research*.
- Gutmann, M. U., Dutta, R., Kaski, S., and Corander, J. (2018). Likelihood-free inference via classification. *Statistics and Computing*, 28(2):411–425.
- Gutmann, M. U. and Hyvärinen, A. (2012). Noise-contrastive estimation of unnormalized statistical models, with applications to natural image statistics. *Journal of Machine Learning Research*, 13(2).
- Hennig, P. and Schuler, C. J. (2012). Entropy search for information-efficient global optimization. *Journal of Machine Learning Research*, 13(6).

- Huszár, F. (2017). Variational inference using implicit distributions. *arXiv preprint arXiv:1702.08235*.
- Järvenpää, M., Gutmann, M. U., Pleska, A., Vehtari, A., and Marttinen, P. (2019). Efficient acquisition rules for model-based approximate Bayesian computation. *Bayesian Analysis*, 14(2):595–622.
- Jarvenpaa, M., Vehtari, A., and Marttinen, P. (2020). Batch simulations and uncertainty quantification in Gaussian process surrogate approximate Bayesian computation. In *Proceedings of the 36th Conference on Uncertainty in Artificial Intelligence*, volume 124, pages 779–788. PMLR.
- Kaji, T. and Ročková, V. (2022). Metropolis-Hastings via classification. *Journal of the American Statistical Association*, pages 1–33.
- Kallenberg, O. (2002). *Foundations of Modern Probability*, volume 2. Springer.
- Kingma, D. P. and Ba, J. (2014). Adam: A method for stochastic optimization. *arXiv preprint arXiv:1412.6980*.
- Kingma, D. P. and Welling, M. (2013). Auto-encoding variational Bayes. *arXiv preprint arXiv:1312.6114*.
- Kingma, D. P. and Welling, M. (2019). An introduction to variational autoencoders. *Foundations and Trends® in Machine Learning*, 12(4):307–392.
- Liang, T. (2021). How well generative adversarial networks learn distributions. *Journal of Machine Learning Research*, 22:1–41.
- Lueckmann, J.-M., Bassetto, G., Karaletsos, T., and Macke, J. H. (2019). Likelihood-free inference with emulator networks. In *Symposium on Advances in Approximate Bayesian Inference*, pages 32–53. PMLR.

- Lueckmann, J.-M., Goncalves, P. J., Bassetto, G., Öcal, K., Nonnenmacher, M., and Macke, J. H. (2017). Flexible statistical inference for mechanistic models of neural dynamics. *Advances in Neural Information Processing Systems*, 30.
- Marjoram, P., Molitor, J., Plagnol, V., and Tavaré, S. (2003). Markov chain Monte Carlo without likelihoods. *Proceedings of the National Academy of Sciences*, 100(26):15324–15328.
- Martin, G. M., McCabe, B. P., Frazier, D. T., Maneesoonthorn, W., and Robert, C. P. (2019). Auxiliary likelihood-based approximate Bayesian computation in state space models. *Journal of Computational and Graphical Statistics*, 28(3):508–522.
- Mescheder, L., Nowozin, S., and Geiger, A. (2017). Adversarial variational Bayes: Unifying variational autoencoders and generative adversarial networks. In *International Conference on Machine Learning*, pages 2391–2400. PMLR.
- Mirza, M. and Osindero, S. (2014). Conditional generative adversarial nets. *arXiv preprint arXiv:1411.1784*.
- Papamakarios, G. and Murray, I. (2016). Fast ε -free inference of simulation models with Bayesian conditional density estimation. In *Advances in Neural Information Processing Systems*, pages 1028–1036.
- Papamakarios, G., Sterratt, D., and Murray, I. (2019). Sequential neural likelihood: Fast likelihood-free inference with autoregressive flows. In *The 22nd International Conference on Artificial Intelligence and Statistics*, pages 837–848. PMLR.
- Ramesh, P., Lueckmann, J.-M., Boelts, J., Tejero-Cantero, Á., Greenberg, D. S., Goncalves, P. J., and Macke, J. H. (2022). GATSBI: Generative adversarial training for simulation-based inference. In *International Conference on Learning Representations*.
- Ranganath, R., Tran, D., Altosaar, J., and Blei, D. (2016). Operator variational inference. *Advances in Neural Information Processing Systems*, 29.

- Schmidt-Hieber, J. (2020). Nonparametric regression using deep neural networks with ReLU activation function. *The Annals of Statistics*, 48(4):1875–1897.
- Sen, B. (2018). A gentle introduction to empirical process theory and applications. *Lecture Notes, Columbia University*.
- Sisson, S. A., Fan, Y., and Beaumont, M. A. (2018). Overview of ABC. In *Handbook of Approximate Bayesian Computation*, pages 3–54. ChapmanBaye and Hall/CRC.
- Sisson, S. A., Fan, Y., and Tanaka, M. M. (2007). Sequential Monte Carlo without likelihoods. *Proceedings of the National Academy of Sciences*, 104(6):1760–1765.
- Stanczuk, J., Etmann, C., Kreuzer, L. M., and Schönlieb, C.-B. (2021). Wasserstein GANs work because they fail (to approximate the Wasserstein distance). *arXiv preprint arXiv:2103.01678*.
- Terrell, G. R. and Scott, D. W. (1992). Variable kernel density estimation. *The Annals of Statistics*, pages 1236–1265.
- Titsias, M. K. and Ruiz, F. (2019). Unbiased implicit variational inference. In *The 22nd International Conference on Artificial Intelligence and Statistics*, pages 167–176. PMLR.
- Tran, D., Ranganath, R., and Blei, D. (2017). Hierarchical implicit models and likelihood-free variational inference. *Advances in Neural Information Processing Systems*, 30.
- Van Handel, R. (2014). Probability in high dimension. Technical report, PRINCETON UNIV NJ.
- Wang, Y., Kaji, T., and Ročková, V. (2022). Approximate Bayesian computation via classification. *The Journal of Machine Learning Research*, 23(1):15837–15885.
- Wilkinson, D. J. (2018). *Stochastic modelling for systems biology*. Chapman and Hall/CRC.
- Zhou, X., Jiao, Y., Liu, J., and Huang, J. (2022). A deep generative approach to conditional sampling. *Journal of the American Statistical Association*, pages 1–12.

A Proofs from Section 4

A.1 Proof of Theorem 1

Proof. We continue denoting $X^{(n)}$ simply by X . Recall the definition of the KL neighborhood

$$B_n(\theta_0; \epsilon) = \{\theta \in \Theta : \text{KL}(P_{\theta_0}^{(n)} \| P_{\theta}^{(n)}) \leq n\epsilon^2, V_{2,0}(P_{\theta_0}^{(n)}, P_{\theta}^{(n)}) \leq n\epsilon^2\}, \quad (27)$$

where $\text{KL}(P_{\theta_0}^{(n)} \| P_{\theta}^{(n)}) = P_{\theta_0}^{(n)} \log[p_{\theta_0}^{(n)}/p_{\theta}^{(n)}]$ and

$$V_{2,0}(P_{\theta_0}^{(n)}, P_{\theta}^{(n)}) = P_{\theta_0}^{(n)} \left| \log[p_{\theta_0}^{(n)}/p_{\theta}^{(n)}] - \text{KL}(P_{\theta_0}^{(n)} \| P_{\theta}^{(n)}) \right|^2. \quad (28)$$

We define an event, for some fixed $C > 0$ and $\epsilon > 0$,

$$\mathcal{A}_n(\epsilon) = \left\{ X : \int_{B_n(\theta_0; \epsilon)} \frac{p_{\theta}^{(n)}(X)}{p_{\theta_0}^{(n)}(X)} \pi(\theta) d\theta > e^{-(1+C)n\epsilon^2} \Pi[B_n(\theta_0; \epsilon)] \right\}.$$

We denote with \mathbb{E} the expectation with respect to $\{(\theta_j, X_j)\}_{j=1}^T$ from the ABC reference table sampled from the joint $\pi(\theta, X)$. For simplicity of notation, we use $\mathbb{E}_{\hat{\beta}_T}$ interchangeably with \mathbb{E} , since it is equivalently accounting for the randomness in $\hat{\beta}_T$. Using the fact that the total variation distance is bounded by 2, we have

$$P_{\theta_0}^{(n)} \mathbb{E}_{\hat{\beta}_T} d_{TV}^2(\nu(X_0), \mu_{\hat{\beta}_T}(X_0)) = \int_{\mathcal{A}_n(\epsilon)} p_{\theta_0}^{(n)}(X_0) \mathbb{E}_{\hat{\beta}_T} d_{TV}^2(\nu(X_0), \mu_{\hat{\beta}_T}(X_0)) dX_0 \quad (29)$$

$$+ 4 \mathbb{P}_{\theta_0}^{(n)}[\mathcal{A}_n^c(\epsilon)]. \quad (30)$$

According to (Ghosal and Van Der Vaart, 2007, Lemma 10), we have $\mathbb{P}_{\theta_0}^{(n)}[\mathcal{A}_n^c(\epsilon)] \leq \frac{1}{C^2 n \epsilon^2}$.

Denoting with $\pi(X) = \int_{\Theta} p_{\theta}^{(n)}(X) \pi(\theta) d\theta$ the marginal likelihood, we can rewrite the term in (29) as

$$\int_{\mathcal{X}} \mathbb{I}_{\mathcal{A}_n(\epsilon)}(X) \pi(X) r(X) \mathbb{E}_{\hat{\beta}_T} d_{TV}^2(\nu(X), \mu_{\hat{\beta}_T}(X)) dX$$

where

$$\frac{1}{r(X)} \equiv \int_{\Theta} \frac{p_{\theta}^{(n)}(X)}{p_{\theta_0}^{(n)}(X)} \pi(\theta) d\theta \geq \int_{B_n(\theta_0; \epsilon)} \frac{p_{\theta}^{(n)}(X)}{p_{\theta_0}^{(n)}(X)} \pi(\theta) d\theta.$$

On the event $\mathcal{A}_n(\epsilon)$, we can thus write

$$r(X) < \frac{e^{(1+C)n\epsilon^2}}{\Pi[B_n(\theta_0; \epsilon)]}.$$

Under the assumption (25), the term in (29) can be upper bounded by

$$e^{(1+C+C_2)n\epsilon^2} \int_{\mathcal{X}} \pi(X) \mathbb{E}_{\hat{\beta}_T} d_{TV}^2(\nu(X), \mu_{\hat{\beta}_T}(X)) dX \leq \frac{e^{(1+C+C_2)n\epsilon^2}}{4} \mathbb{E}_{\hat{\beta}_T} [\text{KL}(\nu \parallel \mu_{\hat{\beta}_T}) + \text{KL}(\mu_{\hat{\beta}_T} \parallel \nu)]. \quad (31)$$

The inequality above stems from the Pinsker's inequality (Van Handel, 2014, Theorem 4.8) and the fact that the joint measures ν and $\mu_{\hat{\beta}_T}$ have the same marginal distribution $\pi(X)$.

In particular, using Fubini's theorem, we can write

$$\begin{aligned} & \int_{\mathcal{X}} \pi(X) \mathbb{E}_{\hat{\beta}_T} d_{TV}^2(\nu(X), \mu_{\hat{\beta}_T}(X)) dX \\ & \leq \frac{1}{4} \int_{\mathcal{X}} \pi(X) \mathbb{E}_{\hat{\beta}_T} [\text{KL}(\nu(X) \parallel \mu_{\hat{\beta}_T}(X)) + \text{KL}(\mu_{\hat{\beta}_T}(X) \parallel \nu(X))] dX \\ & = \frac{1}{4} \mathbb{E}_{\hat{\beta}_T} \int_{\mathcal{X}} \pi(X) \int_{\Theta} \log \frac{\pi(\theta | X)}{\pi_{\hat{\beta}_T}(\theta | X)} [\pi(\theta | X) - \pi_{\hat{\beta}_T}(\theta | X)] d\theta dX \\ & = \frac{1}{4} \mathbb{E}_{\hat{\beta}_T} [\text{KL}(\nu \parallel \mu_{\hat{\beta}_T}) + \text{KL}(\mu_{\hat{\beta}_T} \parallel \nu)] \equiv \frac{1}{4} \mathbb{E}_{\hat{\beta}_T} d_{\text{KL}}^S(\nu, \mu_{\hat{\beta}_T}). \end{aligned}$$

The above inequality is essential for understanding how the average squared total variation distance between the posterior and its approximation (with the average taken with respect to the observed data generating process) can be related to the 'symmetrized' KL divergence $d_{\text{KL}}^S(\nu, \mu_{\hat{\beta}_T})$ between the *joint* distribution and its approximation. We now continue to bound the symmetrized KL divergence. For simplicity, we denote with $\hat{\beta}$ the estimator $\hat{\beta}_T$ in (22). We have the following decomposition, for any ω such that $f_{\omega} \in \mathcal{F}$,

$$\begin{aligned} d_{\text{KL}}^S(\nu, \mu_{\hat{\beta}}) &= \int_{\mathcal{X}} \pi(X) \int_{\Theta} f_{\omega}(\theta, X) [\pi(\theta | X) - \pi_{\hat{\beta}}(\theta | X)] d\theta dX \\ & \quad + \int_{\mathcal{X}} \pi(X) \int_{\Theta} \left[\log \frac{\pi(\theta | X)}{\pi_{\hat{\beta}}(\theta | X)} - f_{\omega}(\theta, X) \right] [\pi(\theta | X) - \pi_{\hat{\beta}}(\theta | X)] d\theta dX \\ & \leq d_{\mathcal{F}}(\nu, \mu_{\hat{\beta}}) + 2 \left\| \log \frac{\pi(\theta | X)}{\pi_{\hat{\beta}}(\theta | X)} - f_{\omega}(\theta, X) \right\|_{\infty}, \end{aligned}$$

where we have used the inequality $\int f g \leq \|f\|_{\infty} \|g\|_1$ and the fact that $\pi(\theta | X)$ and $\pi_{\hat{\beta}}(\theta | X)$ are both non-negative and integrate to one. Then, choosing $f_{\omega} \in \mathcal{F}$ that minimizes the second term we obtain

$$d_{\text{KL}}^S(\nu, \mu_{\hat{\beta}}) \leq 2 \mathcal{A}_1(\mathcal{F}, \mathcal{G}, \hat{\beta}) + d_{\mathcal{F}}(\nu, \mu_{\hat{\beta}}),$$

where $\mathcal{A}_1(\mathcal{F}, \mathcal{G}, \hat{\beta})$ is defined as

$$\mathcal{A}_1(\mathcal{F}, \mathcal{G}, \hat{\beta}) \equiv \inf_{\omega: f_\omega \in \mathcal{F}} \left\| \log \frac{\pi(\theta | X)}{\pi_{\hat{\beta}_T}(\theta | X)} - f_\omega(X, \theta) \right\|_\infty$$

and $\mathcal{A}_1(\mathcal{F}, \mathcal{G}) = \mathbb{E}_{\hat{\beta}} \mathcal{A}_1(\mathcal{F}, \mathcal{G}, \hat{\beta})$ was defined in (23).

We now apply a mild modification of the oracle inequality in (Liang, 2021, Lemma 12). As long as \mathcal{F} and \mathcal{H} are symmetric⁹, then for any β such that $g_\beta \in \mathcal{G}$ we have

$$d_{\mathcal{F}}(\nu, \mu_{\hat{\beta}}) \leq d_{\mathcal{F}}(\mu_\beta, \nu) + 2d_{\mathcal{F}}(\bar{\nu}_T, \nu) + d_{\mathcal{F}}(\bar{\mu}_T^\beta, \mu_\beta) + d_{\mathcal{H}}(\bar{\pi}_T, \pi), \quad (32)$$

where $\bar{\nu}_T$ and $\bar{\mu}_T^\beta$ are the empirical counterparts of ν, μ_β based on T iid samples (ABC reference table $\{(\theta_j, X_j)\}_{j=1}^T$ for ν and $\{(g_\beta(Z_j, X_j), X_j)\}_{j=1}^T$ with $Z_j \stackrel{\text{iid}}{\sim} \pi_Z$ for μ_β). In addition $\bar{\pi}_T$ is the empirical version for the distribution π_Z for Z and $\mathcal{H} = \{h_{\omega, \beta} : h_{\omega, \beta}(Z, X) = f_\omega(X, g_\beta(Z, X))\}$. This oracle inequality can be proved analogously as (Liang, 2021, Lemma 12) the only difference being that due to the conditional structure of our GANs the function class \mathcal{H} is not entirely a composition of networks f_ω and g_β but has a certain nested structure. Similarly as in (Liang, 2021) (proof of Theorem 13), we can write for any β such that $g_\beta \in \mathcal{G}$

$$\begin{aligned} d_{\mathcal{F}}(\mu_\beta, \nu) &\leq B \times d_{TV}(\mu_\beta, \nu) \leq B \sqrt{\frac{1}{4} d_{\text{KL}}^S(\mu_\beta, \nu)} \\ &\leq \frac{B}{\sqrt{2}} \left[\int_{\mathcal{X}} \left\| \log \frac{\pi_\beta(\theta | X)}{\pi(\theta | X)} \right\|_\infty \pi(X) dX \right]^{1/2}. \end{aligned}$$

Choosing β that minimizes the expectation on the right side, we obtain $d_{\mathcal{F}}(\mu_\beta, \nu) \leq \frac{B}{\sqrt{2}} \mathcal{A}_2(\mathcal{G})$, where the term $\mathcal{A}_2(\mathcal{G})$ was defined in (24). Denote with

$$R_T(\mathcal{F}) = E_\varepsilon \sup_{f \in \mathcal{F}} \frac{1}{T} \sum_{j=1}^T \varepsilon_j f(X_j, \theta_j)$$

the Rademacher complexity with $\varepsilon = (\varepsilon_1, \dots, \varepsilon_T)'$ iid Rademacher¹⁰ variables. For the second term in (32), the symmetrization property (see e.g. Lemma 26 in Liang (2021) or

⁹i.e. if $f \in \mathcal{F}$ then also $-f \in \mathcal{F}$

¹⁰taking values $\{-1, +1\}$ with probability 1/2.

Theorem 3.17 in [Sen \(2018\)](#)) yields for $T \geq Pdim(\mathcal{F})$

$$\mathbb{E} d_{\mathcal{F}}(\bar{\nu}_T, \nu) \leq 2 \mathbb{E} R_T(\mathcal{F}) \leq \tilde{C} \times B \sqrt{\frac{Pdim(\mathcal{F}) \log T}{T}}$$

for some $\tilde{C} > 0$, where $Pdim(\mathcal{F})$ is the pseudo-dimension of the function class \mathcal{F} (Definition 2 in [\(Bartlett et al., 2017\)](#)). The second inequality follows, for example, from Lemma 29 in [\(Liang, 2021\)](#). The bounds on $\mathbb{E} d_{\mathcal{H}}(\bar{\pi}_T, \pi)$, and $\mathbb{E} d_{\mathcal{F}}(\bar{\mu}_T^{\beta}, \mu_{\beta})$ in [\(32\)](#) are analogous. Putting the pieces together from the oracle inequality in [\(32\)](#) we can upper-bound $P_{\theta_0}^{(n)} \mathbb{E} d_{TV}^2(\nu(X_0), \mu_{\hat{\beta}_T}(X_0))$ with

$$\frac{1}{C^2 n \varepsilon^2} + \frac{e^{(1+C+C_2)n\varepsilon^2}}{4} \left[2\mathcal{A}_1(\mathcal{F}, \mathcal{G}) + \frac{B}{\sqrt{2}} \mathcal{A}_2(\mathcal{G}) + 4\tilde{C} B \sqrt{\frac{\log T}{T}} (Pdim(\mathcal{F}) \vee Pdim(\mathcal{H}))^{1/2} \right]$$

which yields the desired statement. \square

A.2 Proof of Corollary 1

Proof. We continue to use the shorthand notation X for $X^{(n)}$ and $\hat{\beta}$ for $\hat{\beta}_T$. Denote with $\tilde{\pi}(\theta)$ the proposal distribution. Then, the posterior $\tilde{\pi}(\theta | X)$ under $\tilde{\pi}(\theta)$ satisfies

$$\pi(\theta | X) = \tilde{\pi}(\theta | X) \times R(X) \times r(\theta), \quad \text{where} \quad R(X) = \frac{\tilde{\pi}(X)}{\pi(X)} \quad \text{and} \quad r(\theta) = \frac{\pi(\theta)}{\tilde{\pi}(\theta)}. \quad (33)$$

Our reconstruction in [Algorithm 2](#) works by first approximating the joint distribution $\tilde{\pi}(\theta, X)$ and then reweighting by the prior ratio, namely

$$\pi_{\hat{\beta}}(\theta | X) = \tilde{\pi}_{\hat{\beta}}(\theta | X) \times R(X) \times r(\theta), \quad (34)$$

where $\hat{\beta}$ has been learned by B-GAN ([Algorithm 1](#)) by matching the joint $\tilde{\pi}(\theta, X) = \tilde{\pi}(\theta | X)\tilde{\pi}(X)$ under the prior $\tilde{\pi}(\theta)$. We denote the joint measure with this density by $\tilde{\nu}$. Denote with $\mu_{\hat{\beta}_T}(X)$ the approximating conditional measure with a density [\(34\)](#). We can apply the same steps as in the proof of [Theorem 1](#) until the step in [\(31\)](#). Similarly, we denote with $\tilde{\mathbb{E}}$ the expectation with respect to $\{(\theta_j, X_j)\}_{j=1}^T$ from the ABC reference table sampled from the joint $\tilde{\pi}(\theta, X)$, and we use $\tilde{\mathbb{E}}_{\hat{\beta}_T}$ interchangeably with $\tilde{\mathbb{E}}$. The next steps will have minor modifications. Notice that

$$\log \frac{\pi(\theta | X)}{\pi_{\hat{\beta}}(\theta | X)} = \log \frac{\tilde{\pi}(\theta | X)}{\tilde{\pi}_{\hat{\beta}}(\theta | X)}$$

and thereby

$$\begin{aligned}
& \int_{\mathcal{X}} \pi(X) \tilde{\mathbb{E}}_{\hat{\beta}} d_{TV}^2(\nu(X), \mu_{\hat{\beta}_T}(X)) dX \\
& \leq \frac{1}{4} \int_{\mathcal{X}} \pi(X) \tilde{\mathbb{E}}_{\hat{\beta}} \left[\text{KL}(\nu(X) \parallel \mu_{\hat{\beta}}(X)) + \text{KL}(\mu_{\hat{\beta}}(X) \parallel \nu(X)) \right] dX \\
& = \frac{1}{4} \tilde{\mathbb{E}}_{\hat{\beta}} \int_{\mathcal{X}} \pi(X) \int_{\Theta} \log \frac{\pi(\theta | X)}{\pi_{\hat{\beta}}(\theta | X)} [\pi(\theta | X) - \pi_{\hat{\beta}}(\theta | X)] d\theta dX \\
& = \frac{1}{4} \tilde{\mathbb{E}}_{\hat{\beta}} \int_{\mathcal{X}} \tilde{\pi}(X) \int_{\Theta} r(\theta) \log \frac{\pi(\theta | X)}{\pi_{\hat{\beta}}(\theta | X)} [\tilde{\pi}(\theta | X) - \tilde{\pi}_{\hat{\beta}}(\theta | X)] d\theta dX \\
& \equiv \frac{1}{4} \tilde{\mathbb{E}}_{\hat{\beta}} d_{\text{KL}}^S(\tilde{\nu}, \tilde{\mu}_{\hat{\beta}}).
\end{aligned}$$

Using similar arguments as in the proof of Theorem 1, we have the following decomposition, for any ω such that $f_{\omega} \in \mathcal{F}$,

$$\begin{aligned}
d_{\text{KL}}^S(\tilde{\nu}, \tilde{\mu}_{\hat{\beta}}) &= \int_{\mathcal{X}} \tilde{\pi}(X) \int_{\Theta} f_{\omega}(\theta, X) [\tilde{\pi}(\theta | X) - \tilde{\pi}_{\hat{\beta}}(\theta | X)] d\theta dX \\
& \quad + \int_{\mathcal{X}} \tilde{\pi}(X) \int_{\Theta} \left[r(\theta) \log \frac{\pi(\theta | X)}{\pi_{\hat{\beta}}(\theta | X)} - f_{\omega}(\theta, X) \right] [\tilde{\pi}(\theta | X) - \tilde{\pi}_{\hat{\beta}}(\theta | X)] d\theta dX \\
& \leq d_{\mathcal{F}}(\tilde{\nu}, \tilde{\mu}_{\hat{\beta}}) + 2 \left\| r(\theta) \log \frac{\pi(\theta | X)}{\pi_{\hat{\beta}}(\theta | X)} - f_{\omega}(\theta, X) \right\|_{\infty}.
\end{aligned}$$

The rest of the proof is analogous. The only difference is that $\hat{\beta}$ now minimizes the empirical version of $d_{\mathcal{F}}(\tilde{\nu}, \tilde{\mu}_{\hat{\beta}})$ under the proposal distribution $\tilde{\pi}(\theta)$.

A.3 Motivation for the Sequential Refinement

Remark 4 (2step Motivation). *For the proposal distribution $\tilde{\pi}(\theta)$, using similar arguments as in the proof of Theorem 1, the TV distance of the posterior at X_0 (not averaged over $P_{\theta_0}^{(n)}$) can be upper-bounded by*

$$4 d_{TV}^2(\nu(X_0), \mu_{\hat{\beta}}(X_0)) \leq 2 \mathcal{A}_1(\mathcal{F}, \mathcal{G}, X_0) + \frac{B}{\sqrt{2}} \mathcal{A}_2(\mathcal{G}) + 4\tilde{C} B \sqrt{\frac{\log T \times Pmax}{T}} + A_3(\tilde{\pi})$$

where $\mathcal{A}_1(\mathcal{F}, \mathcal{G}, X_0) \equiv \sup_{\beta: g_{\beta} \in \mathcal{G}} \inf_{\omega: f_{\omega} \in \mathcal{F}} \left\| \log \frac{\pi(\theta | X_0)}{\pi_{\beta}(\theta | X_0)} - \frac{f_{\omega}(X_0, \theta)}{r(\theta)} \right\|$ is the discriminability evaluated at X_0 (as opposed to (23)) and where

$$A_3(\tilde{\pi}) = 2 \int_{\mathcal{X}} \tilde{\pi}(X) \left[\|f_{\omega}(X_0, \theta) - f_{\omega}(X, \theta)\|_{\infty} + B \|g_{\hat{\beta}}(\theta)(X) - g_{\hat{\beta}}(\theta)(X_0)\|_1 \right] dX$$

and $g_{\hat{\beta}}(\theta)(X) \equiv \pi(\theta | X) - \pi_{\hat{\beta}}(\theta | X)$. This decomposition reveals how the TV distance can be related to discriminability around X_0 and an average discrepancy between the true and approximated posterior densities relative to their value at X_0 where the average is taken over the marginal $\tilde{\pi}(X)$. These averages will be smaller since the marginal $\tilde{\pi}(X)$ produces datasets more similar to X_0 . For example, an approximation to the the posterior predictive distribution $\tilde{\pi}(X) = \int_{\mathcal{X}} p_{\theta}^{(n)}(X) \pi_{\hat{\beta}}(\theta | X_0)$ where $\hat{\beta}$ has been learned by B-GAN (Algorithm 1) is likely to yield datasets similar to X_0 , thereby producing a tighter upper bound than a flat prior.

We provide clarifications of the calculations and reasoning in Remark 4. We assume that a prior distribution $\tilde{\pi}(\theta)$ has been used in the ABC reference table that yields the marginal $\tilde{\pi}(X) = \int_{\mathcal{X}} p_{\theta}^{(n)}(X) \tilde{\pi}(\theta) d\theta$. Recall the definition of the reweighted posterior reconstruction in (34) and (33). Denote with

$$g_{\hat{\beta}}(\theta)(X) \equiv \pi(\theta | X) - \pi_{\hat{\beta}}(\theta | X) = R(X) \times r(\theta) \times [\tilde{\pi}(\theta | X) - \tilde{\pi}_{\hat{\beta}}(\theta | X)]$$

the difference between true and approximated posteriors at X , where $\hat{\beta}$ has been trained using the proposal $\tilde{\pi}(\theta)$ and where $R(X) = \tilde{\pi}(X)/\pi(X)$ and $r(\theta) = \pi(\theta)/\tilde{\pi}(\theta)$. Using similar arguments as in the proof of Theorem 1, the squared TV distance of the posterior

and its approximation satisfies, for any element $f_\omega \in \mathcal{F} = \{f : \|f\|_\infty \leq B\}$,

$$\begin{aligned}
4 d_{TV}^2 \left(\nu(X_0), \mu_{\hat{\beta}}(X_0) \right) &\leq \int_{\Theta} \log \frac{\pi(\theta | X_0)}{\pi_{\hat{\beta}}(\theta | X_0)} g_{\hat{\beta}}(\theta)(X_0) d\theta \\
&= \int_{\Theta} \left[\log \frac{\pi(\theta | X_0)}{\pi_{\hat{\beta}}(\theta | X_0)} - \frac{f_\omega(X_0, \theta)}{r(\theta)} \right] g_{\hat{\beta}}(\theta)(X_0) d\theta \\
&\quad + \int_{\mathcal{X}} \pi(X) \int_{\Theta} \frac{f_\omega(X, \theta)}{r(\theta)} g_{\hat{\beta}}(\theta)(X_0) d\theta dX \\
&\quad + \int_{\mathcal{X}} \frac{\pi(X)}{r(\theta)} \int_{\Theta} [f_\omega(X_0, \theta) - f_\omega(X, \theta)] g_{\hat{\beta}}(\theta)(X_0) d\theta dX \\
&\leq 2 \inf_{\omega} \left\| \log \frac{\pi(\theta | X_0)}{\pi_{\hat{\beta}}(\theta | X_0)} - \frac{f_\omega(X_0, \theta)}{r(\theta)} \right\|_{\infty} + d_{\mathcal{F}}(\tilde{\nu}, \tilde{\mu}_{\hat{\beta}}) \\
&\quad + 2 \int_{\mathcal{X}} \tilde{\pi}(X) \|f_\omega(X_0, \theta) - f_\omega(X, \theta)\|_{\infty} dX \\
&\quad + 2B \times \int_{\mathcal{X}} \tilde{\pi}(X) \left\| \frac{g_{\hat{\beta}}(\theta)(X)}{R(X)r(\theta)} - \frac{g_{\hat{\beta}}(\theta)(X_0)}{R(X_0)r(\theta)} \right\|_1 dX.
\end{aligned}$$

The term $d_{\mathcal{F}}(\tilde{\nu}, \tilde{\mu}_{\hat{\beta}})$ can be bounded as in the proof of Corollary 1 by

$$\frac{B}{\sqrt{2}} \tilde{\mathcal{A}}_2(\mathcal{G}) + 4\tilde{C} B \sqrt{\frac{\log T \times Pmax}{T}}$$

Compared to Corollary 1, the upper bound on $d_{TV}^2(\nu(X_0), \mu_{\hat{\beta}}(X_0))$ now involves the discriminability *evaluated at* X_0 (not averaged over the marginal $\tilde{\pi}(X)$), i.e.

$$\mathcal{A}_1(\mathcal{F}, \mathcal{G}, X_0) \equiv \sup_{\beta: g_\beta \in \mathcal{G}} \inf_{\omega: f_\omega \in \mathcal{F}} \left\| \log \frac{\pi(\theta | X_0)}{\pi_\beta(\theta | X_0)} - \frac{f_\omega(X_0, \theta)}{r(\theta)} \right\|.$$

The additional two terms in the upper bound involve integration over $\tilde{\pi}(X)$.

□

A.4 Clarification of Remark 3

With $\varepsilon_n = O(1/\sqrt{n})$ we need to verify that for some suitable choice of $C_n \rightarrow \infty$ we have as $n \rightarrow \infty$

$$A_1(\mathcal{F}, \mathcal{G}) = o(e^{-C_n}) \tag{35}$$

$$A_2(\mathcal{G}) = o(e^{-C_n}) \tag{36}$$

$$\frac{\log T}{T} \times [Pdim(\mathcal{F}) \vee Pdim(\mathcal{H})] = o(e^{-2C_n}) \tag{37}$$

for T that is large enough, i.e. $T \geq Pdim(\mathcal{F}) \vee Pdim(\mathcal{H})$. The term $\mathcal{A}_2(\mathcal{G})$ equals zero from our assumption of representability of $\pi(\theta, X) = \pi_{g_{\beta_0}}(\theta, X)$ for $g_{\beta_0} \in \mathcal{G}$, which verifies (36). We assume that $X^{(n)}$ is a stacked vector of n observed vectors of length q , not necessarily iid, and denote $d^* = d + nq$. Using leaky ReLU networks and assuming representability, for any β such that $g_\beta \in \mathcal{G}$ the log posterior ratio $r_\beta(\theta, X^{(n)}) = \log \frac{\pi(\theta | X^{(n)})}{\pi_\beta(\theta | X^{(n)})}$ is continuous and, due to boundedness of the network weights, satisfies

$$0 < \underline{C} \leq r_\beta(\theta, X^{(n)}) \leq \bar{C} < \infty$$

for any fixed d^* . With large enough T and setting $E = [-\log T, \log T]^{d^*}$ and $R = \log T$, Lemma 3 yields that there exists a ReLU network $f_\omega \in \mathcal{F}$ with a width

$$W = 3^{d^*+3} \max\{d^* \lfloor N^{1/d^*} \rfloor, N + 1\}$$

and depth $L = 12 \log T + 14 + 2d^*$ such that

$$\mathcal{A}_1(\mathcal{F}, \mathcal{G}) \leq \sup_{\beta: g_\beta \in \mathcal{G}} \inf_{\omega: f_\omega \in \mathcal{F}} \|r_\beta(\theta, X^{(n)}) - f_\omega(X^{(n)}, \theta)\|_{L^\infty(E)} \leq 19\sqrt{d^*} \omega_f^E(2(\log T)^{1-2/d^*} N^{-2/d^*}),$$

where ω_f^E is the modulus of continuity of $f(t)$ satisfying $\omega_f^E(t) \rightarrow 0$ as $t \rightarrow 0^+$. Choosing N such that $2^{d^*/2}(\log T)^{d^*/2-1} = o(N)$ as $T \rightarrow \infty$, the right-hand side above goes to zero for any fixed $d^* = d + nq$. For each n , we can find T large enough (depending on the modulus of continuity) such that $\mathcal{A}_1(\mathcal{F}, \mathcal{G})e^{Cn} \sqrt{d^*} \leq \eta_n$ for some $\eta_n = o(1)$, yielding (35). The smallest T that satisfies this will be denoted with T_n .

In order to verify (37), Theorem 14.1 in [Anthony and Bartlett \(1999\)](#) and Theorem 6 in [Bartlett et al. \(2017\)](#) show that for piecewise linear activation functions (including ReLU and leaky ReLU) there exist constants $c, C > 0$ such that

$$c \times SL \log(S/L) \leq Pdim(\mathcal{F}) \leq C \times SL \log S,$$

where \mathcal{F} is a class of discriminator networks with L layers and S parameters. Since elements in \mathcal{H} can be regarded as sparse larger neural networks with $L + L^*$ layers, $S + S^*$ parameters and piece-wise linear activations, we have

$$Pdim(\mathcal{F}) \vee Pdim(\mathcal{H}) \leq C \times (S + S^*)(L + L^*) \log(S + S^*).$$

Our assumption $T \geq Pdim(\mathcal{F}) \vee Pdim(\mathcal{H})$ will thus be satisfied, for instance, when

$$T > C \times (S + S^*)(L + L^*) \log(S + S^*). \quad (38)$$

Choosing $N = \lfloor 2^{d^*/2}(\log T)^{d^*/2} \rfloor$, which satisfies the requirement $2^{d^*/2}(\log T)^{d^*/2-1} = o(N)$ as $T \rightarrow \infty$, yields

$$W = 3^{d^*+3} \max\{d^* \lfloor N^{1/d^*} \rfloor, N + 1\} = 3^{d^*+3} \lfloor 2^{d^*/2}(\log T)^{d^*/2} + 1 \rfloor \quad (39)$$

for a sufficiently large n (and thereby d^*). Recall that in the feed-forward neural networks, the total number of parameters $S = \sum_{l=0}^{L-1} [w_l(w_l + 1)]$ satisfies $S \leq LW(W + 1)$. For any fixed d^* (and thereby n), assuming $L = 12 \log T + 14 + 2d^*$ as before and W as in (39), we define $T(d^*)$ as the smallest T that satisfies

$$C \times [LW(W + 1) + S^*](L + L^*) \log[LW(W + 1) + S^*] \leq \frac{T}{\log T} \times e^{-2C_n} \times \eta_n$$

for some $\eta_n = o(1)$. Any $T > T(d^*)$ satisfies $T > Pdim(\mathcal{F}) \vee Pdim(\mathcal{H})$ and $e^{2C_n} \frac{\log T}{T} [Pdim(\mathcal{F}) \vee Pdim(\mathcal{H})] \leq \eta_n$. With $T \geq \max\{T_n, T(d^*)\}$, the condition (37) is verified.

Lemma 3. (*Zhou et al., 2022, Lemma B5*) *Let f be a uniformly continuous function defined on $E \subset [-R, R]^d$. For any $L, N \in \mathbb{N}^+$, there exists a ReLU network function f_ϕ with width $3^{d+3} \max\{d \lfloor N^{1/d} \rfloor, N + 1\}$ and depth $12L + 14 + 2d$ such that*

$$\|f - f_\phi\|_{L^\infty(E)} \leq 19\sqrt{d}\omega_f^E(2RN^{-2/d}L^{-2/d}),$$

where $\omega_f^E(t)$ is the modulus of continuity of $f(t)$ satisfying $\omega_f^E(t) \rightarrow 0$ as $t \rightarrow 0^+$.

A.5 Theory for Adversarial Variational Bayes

Theorem 2. *Let $\hat{\beta}_T$ be as in (40) where $\mathcal{F} = \{f : \|f\|_\infty \leq B\}$ for some $B > 0$. Denote with \mathbb{E} the expectation with respect to $\{Z_j\}_{j=1}^T$ in the reference table. Assume that the prior satisfies (25). Then for $T \geq Pdim(\mathcal{F} \circ \mathcal{G})$ we have for any $C_n > 0$*

$$P_{\theta_0}^{(n)} \mathbb{E} d_{TV}^2(\nu(X_0), \mu_{\hat{\beta}_T}(X_0)) \leq \mathcal{D}_n^T(\mathcal{F}, \mathcal{G}, \varepsilon_n, C_n),$$

where

$$D_n^T(\mathcal{F}, \mathcal{G}, \varepsilon_n, C_n) = \frac{\mathcal{A}_3(\mathcal{F}, \mathcal{G})}{2} + \frac{1}{C_n^2 n \varepsilon_n^2} + \frac{1}{2} \tilde{C} \sqrt{\frac{\log T}{T} P \dim(\mathcal{F} \circ \mathcal{G})} + \frac{e^{(1+C_2+C_n)n\varepsilon_n^2}}{4} \frac{B}{\sqrt{2}} \mathcal{A}_2(\mathcal{G})$$

for some $\tilde{C} > 0$ where $\mathcal{A}_2(\mathcal{G})$ was defined in (24) and where

$$\mathcal{A}_3(\mathcal{F}, \mathcal{G}) = P_{\theta_0}^{(n)} \mathbb{E} \left\| \log \frac{\pi_{\hat{\beta}_T}(\theta | X_0)}{\pi(\theta | X_0)} - f_{\omega(\hat{\beta}_T)}(X_0, \theta) \right\|_{\infty}.$$

Here \mathbb{E} account for the nested randomness in the estimation process of $\omega(\hat{\beta}_T)$ and $\hat{\beta}_T$.

Proof. We denote with \bar{E} the expectation with respect to the empirical distribution. Because the class \mathcal{F} is symmetrical (i.e. $f \in \mathcal{F}$ implies $-f \in \mathcal{F}$), the adversarial variational Bayes estimator is defined as

$$\hat{\beta}_T = \arg \min_{\beta: g_{\beta} \in \mathcal{G}} \left[\bar{E}_{Z \sim \pi_Z} f_{\omega(\beta)}(X_0, g_{\beta}(Z, X_0)) - E_{\theta \sim \pi(\theta | X_0)} f_{\omega(\beta)}(X_0, \theta) \right] \quad (40)$$

where

$$\omega(\beta) = \arg \max_{\omega: f_{\omega} \in \mathcal{F}} \left[\bar{E}_{Z \sim \pi_Z, X \sim \pi(X)} f_{\omega}(X, g_{\beta}(Z, X)) - \bar{E}_{(\theta, X) \sim \pi(\theta, X)} f_{\omega}(X, \theta) \right].$$

Note that the (stochastic) gradient descent update for β , conditioning on the most recent value of ω , *does not* involve the second term $E_{\theta \sim \pi(\theta | X_0)} f_{\omega(\beta)}(\theta, X_0)$ in (40) because it does not depend on β . The minimization occurs only over the first term. We obtain theoretical results for $\hat{\beta}_T$ and note that our Algorithm 3 targets this estimator. In the sequel, we denote $\hat{\beta}_T$ simply by $\hat{\beta}$ and use the notation $\pi_{\beta}(\theta, X) = \pi_{\beta}(\theta | X)\pi(X)$ for the joint generator model. Using the Pinsker inequality we obtain

$$\begin{aligned} P_{\theta_0}^{(n)} \mathbb{E} 4 d_{TV}^2(\nu(X_0), \mu_{\hat{\beta}}(X_0)) &\leq P_{\theta_0}^{(n)} \mathbb{E} \int_{\Theta} \log \frac{\pi(\theta | X_0)}{\pi_{\hat{\beta}}(\theta | X_0)} [\pi(\theta | X_0) - \pi_{\hat{\beta}}(\theta | X_0)] d\theta \\ &\leq P_{\theta_0}^{(n)} \mathbb{E} 2 \left\| \log \frac{\pi_{\hat{\beta}}(\theta | X_0)}{\pi(\theta | X_0)} - f_{\omega(\hat{\beta})}(X_0, \theta) \right\|_{\infty} \\ &\quad + P_{\theta_0}^{(n)} \mathbb{E} d_{\hat{\beta}}(\nu_{\hat{\beta}}(X_0), \mu(X_0)), \end{aligned}$$

where we define (for any $\beta, \tilde{\beta}$ such that $g_{\beta} \in \mathcal{G}$ and $g_{\tilde{\beta}} \in \mathcal{G}$)

$$d_{\tilde{\beta}}(\nu_{\beta}(X), \mu(X)) \equiv E_{\theta \sim \pi_{\beta}(\theta | X)} f_{\omega(\tilde{\beta})}(X, \theta) - E_{\theta \sim \pi(\theta | X)} f_{\omega(\tilde{\beta})}(X, \theta).$$

From the definition of (40) and since $\mathcal{F} \circ \mathcal{G}$ is symmetrical, we have for any realization X_0 and for any β

$$\begin{aligned}
d_{\hat{\beta}}(\nu_{\hat{\beta}}(X_0), \mu(X_0)) &= d_{\hat{\beta}}(\nu_{\hat{\beta}}(X_0), \bar{\nu}_{\hat{\beta}}(X_0)) + d_{\hat{\beta}}(\bar{\nu}_{\hat{\beta}}(X_0), \mu(X_0)) \\
&\leq d_{\hat{\beta}}(\nu_{\hat{\beta}}(X_0), \bar{\nu}_{\hat{\beta}}(X_0)) + d_{\beta}(\bar{\nu}_{\beta}(X_0), \mu(X_0)) \\
&\leq d_{\mathcal{F}}(\nu_{\hat{\beta}}(X_0), \bar{\nu}_{\hat{\beta}}(X_0)) + d_{\beta}(\bar{\nu}_{\beta}(X_0), \nu_{\beta}(X_0)) + d_{\beta}(\nu_{\beta}(X_0), \mu(X_0)) \\
&\leq 2d_{\mathcal{F} \circ \mathcal{G}}(\pi_Z, \bar{\pi}_Z) + d_{\beta}(\nu_{\beta}(X_0), \mu(X_0)).
\end{aligned} \tag{41}$$

Next, using the same arguments as in the proof of Theorem 1, we obtain

$$P_{\theta_0}^{(n)} \mathbb{E} d_{\beta}(\nu_{\beta}(X_0), \mu(X_0)) \leq 4 \mathbb{P}_{\theta_0}^{(n)}[\mathcal{A}_n^c(\epsilon)] + e^{(1+C_n+C_2)n\epsilon^2} \mathbb{E} \int_{\mathcal{X}} d_{\beta}(\nu_{\beta}(X), \mu(X)) \pi(X) dX$$

Since $\|f_{\omega(\beta)}\|_{\infty} \leq B$, we have for any β

$$\begin{aligned}
E_X d_{\beta}(\mu_{\beta}(X), \nu(X)) &= \int_{\mathcal{X}} \pi(X) \int_{\Theta} f_{\omega(\beta)}(X, \theta) [\pi(\theta | X) - \pi_{\beta}(\theta | X)] d\theta dX \\
&\leq B \times E_X d_{TV}(\mu_{\beta}(X), \nu(X)) \\
&\leq \frac{B}{\sqrt{2}} E_X \sqrt{\left\| \log \frac{\pi(\theta | X)}{\pi_{\beta}(\theta | X)} \right\|_{\infty}}.
\end{aligned}$$

In the sequel, we choose β which minimizes this term. Next, using the symmetrization techniques as before in the proof of Theorem 1 and denoting with \mathbb{E} the expectation with respect to $\{Z_j\}_{j=1}^T$, we have

$$d_{\mathcal{F} \circ \mathcal{G}}(\pi_Z, \bar{\pi}_Z) \leq \mathbb{E} \mathcal{R}_n(\mathcal{F} \circ \mathcal{G}) \leq \tilde{C} \sqrt{\frac{\log T}{T} Pdim(\mathcal{F} \circ \mathcal{G})}.$$

Putting the pieces together, we obtain an upper bound $D_n^T(\mathcal{F}, \mathcal{G}, \epsilon_n, C_n)$ for $P_{\theta_0}^{(n)} \mathbb{E} d_{TV}^2(\nu(X_0), \mu_{\hat{\beta}_T}(X_0))$.

B More on Adversarial Variational Bayes

B.1 B-GAN-VB Algorithm

The VB algorithm reported in the main paper follows the scheme in Table 3. We have also considered variants initializing the method on top of Algorithm 2 (more discussion in Section B.3). Figure 6 includes an example of performance of Algorithm 3 on another realization of Example 1.

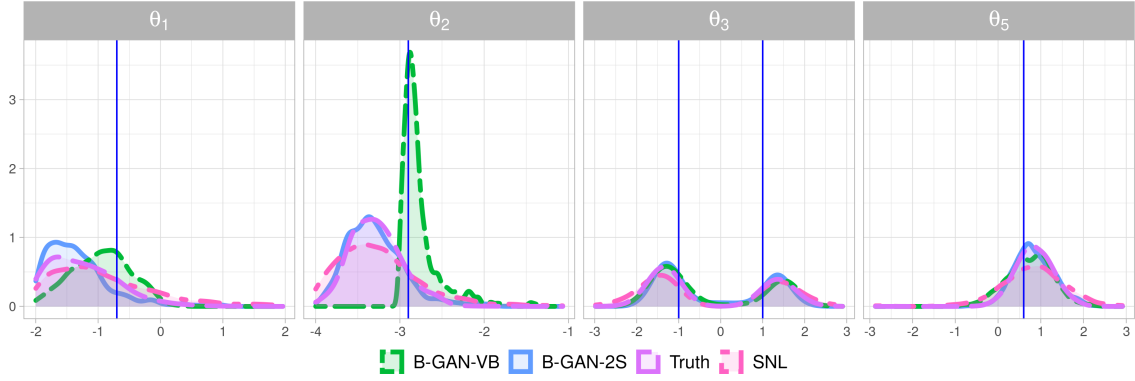


Figure 6: Posterior densities under the Gaussian model (another repetition). The true parameter is $\theta_0 = (-0.7, -2.9, -1.0, -0.9, 0.6)'$, while the signs of θ_3 and θ_4 are not identifiable.

Algorithm 3 <i>Adversarial Variational Bayes (Wasserstein Version)</i>	
INPUT	
Prior $\pi(\theta)$, observed data X_0 and noise distribution $\pi_Z(z)$	
Training	
Pilot Run	
Apply Algorithm 2 with $\pi(\theta)$ to learn $\hat{g}_{pilot}(\cdot)$ Initialize critic network $\omega^{(0)} = 0$ and the generator network at $g_{\beta^{(0)}} = g_{pilot}(\cdot)$	
Reference Table	
Generate pairs $\{(X_j, \theta_j)\}_{j=1}^T$ where $\theta_j = \hat{g}_{pilot}(Z_j, X_0)$ for $Z_j \sim \pi_Z$ and $X_j \sim P_{\theta_j}^{(n)}$.	
WGAN Training	
For $t = 1, \dots, N$:	
Critic Update (N_{critic} steps): Same as in Critic Update of Algorithm 1	
Generator Update (single step)	
Generate noise $Z_j \sim \pi_Z(z)$ for $j = 1, \dots, N$.	
Update $\beta^{(t)}$ by applying stochastic gradient descent on (18).	
Posterior Simulation	
Simulate $\{Z_i\}_{i=1}^M \stackrel{iid}{\sim} \pi_Z(z)$ and set $\tilde{\theta}_i = g_{\beta^{(N)}}(Z_i, X_0)$.	
Estimate \hat{w}_i using either (9) or (10).	
OUTPUT	
Pairs of posterior samples and weights $(\tilde{\theta}_1, \hat{w}_1), \dots, (\tilde{\theta}_M, \hat{w}_M)$	

B.2 Comparisons of Different VB Implementations

In this section, we provide more implementation details on alternative VB variants mentioned briefly in Section 3 and we look into their performance on the toy example in

Example 1.

The JS-Version. The maximization of the ELBO in (14) can be achieved by playing an adversarial game between the discriminator and the generator. While the generator is directly targeted at the ELBO itself, the discriminator tries to distinguish between the two conditionals $q_{g_\beta}(\theta | X_0)$ and $\pi(\theta | X_0)$ by learning the differences between the two joints $\pi_{g_\beta}(\theta, X)$ and $\pi(\theta, X)$. Starting from $(\phi^{(0)}, \beta^{(0)})$, the empirical version of this game involves again the ABC reference table $\{(\theta_j, X_j)\}_{j=1}^T$ sampled from the joint $\pi(\theta, X)$ and noise variables $\{Z_j\}_{j=1}^T$ sampled from $\pi_Z(\cdot)$ to iteratively:

- update $\phi^{(t+1)}$ to learn the density ratio of joint distributions, given $\beta^{(t)}$,

$$\phi^{(t+1)} = \arg \max_{\phi: d_\phi \in \mathcal{D}} \sum_{j=1}^T \left\{ \log d_\phi(X_j, \theta_j) + \log \left[1 - d_\phi(X_j, g_{\beta^{(t)}}(Z_j, X_j)) \right] \right\} \quad (42)$$

- update $\beta^{(t+1)}$ to maximize the evidence lower bound, given $\phi^{(t+1)}$,

$$\beta^{(t+1)} = \arg \min_{\beta: g_\beta \in \mathcal{G}} \sum_{j=1}^T \log \left[\frac{1 - d_{\phi^{(t+1)}}(X_0, g_\beta(Z_j, X_0))}{d_{\phi^{(t+1)}}(X_0, g_\beta(Z_j, X_0))} \right]. \quad (43)$$

After convergence, the procedure outputs $\hat{\beta}_T$ and a neural sampler $g_{\hat{\beta}_T}(Z, X_0)$ which generates samples from an approximate posterior $\pi(\theta | X_0)$

$$\tilde{\theta}_j = g_{\hat{\beta}_T}(Z_j, X_0) \quad \text{where} \quad Z_j \sim \pi_Z(\cdot) \quad \text{for} \quad j = 1, \dots, M. \quad (44)$$

One then needs to compute the gradient of (43) to update $\beta^{(t+1)}$, which is implicitly dependent of $\beta^{(t)}$, since $\phi^{(t)}$ depends on $\beta^{(t)}$. It helps to note that, for any $\beta^{(t)}$ (t^{th} iteration of the gradient descent) we have

$$\frac{\partial}{\partial \beta} E_{q_\beta} \log \left(1 - d_{g_\beta}(\theta, X_0) \right) \Big|_{\beta=\beta^{(t)}} = \frac{\partial}{\partial \beta} E_{q_\beta} \log \left(1 - d_{g_{\beta^{(t)}}}(\theta, X_0) \right) \Big|_{\beta=\beta^{(t)}}.$$

The only difference above is that the dependence on β inside the expectation can be ignored. This has huge computational benefits because one can then approximate the integral using the reparametrization trick [Kingma and Welling \(2013\)](#). Note that the variational lower bound (14) depends on the observed data vector X_0 . While the discriminator is trained solely on the fake data, the generator is trained on the observed data X_0 given the returned discriminator.

Another Wasserstein Version. To minimize the Wasserstein loss specified in (16), we can again approximate the density ratio using classification on the joint distributions. This Wasserstein version will have one additional step for learning this density ratio. Starting from $(\phi^{(0)}, \beta^{(0)}, \omega^{(0)})$, the empirical version of this game involves again the ABC reference table $\{(\theta_j, X_j)\}_{j=1}^T$ sampled from the joint $\pi(\theta, X)$ and noise variables $\{Z_j\}_{j=1}^T$ sampled from $\pi_Z(\cdot)$ to iteratively:

- update $\phi^{(t+1)}$ to learn the ratio of the joint distributions as in (42)
- update $\omega^{(t+1)}$ to approximate the Wasserstein distance, given $\phi^{(t+1)}$ and $\beta^{(t)}$,

$$\omega^{(t+1)} = \arg \max_{\omega} \left| \sum_{j=1}^T \left[\frac{1 - d_{\phi^{(t+1)}}(X_0, g_{\beta^{(t)}}(Z_j, X_0))}{d_{\phi^{(t+1)}}(X_0, g_{\beta^{(t)}}(Z_j, X_0))} - 1 \right] f_{\omega}(g_{\beta^{(t)}}(Z_j, X_0)) \right| \quad (45)$$

- update $\beta^{(t+1)}$ to minimize the approximate Wasserstein distance, given $\phi^{(t+1)}$ and $\omega^{(t+1)}$,

$$\beta^{(t+1)} = \arg \min_{\beta} \sum_{j=1}^T \left[\frac{1 - d_{\phi^{(t+1)}}(X_0, g_{\beta}(Z_j, X_0))}{d_{\phi^{(t+1)}}(X_0, g_{\beta}(Z_j, X_0))} - 1 \right] f_{\omega^{(t+1)}}(g_{\beta}(Z_j, X_0)) \quad (46)$$

What is curious about this version is that the critic function f_{ω} is lower-dimensional, operating *only* in the Θ space as opposed to $(\mathcal{X} \times \Theta)$ space.

Example 3 (Toy Example Continued). *We investigate the performance of the three different VB variants on the toy example studied in Example 1 and Example 2. We refer to the JS version of adversarial VB updates in (42) and (43) as JS-VB, the VB updates in (45) and (46) under the Wasserstein distance loss in (16) as W-VB, and the VB updates using Algorithm 3 as B-GAN-VB. For both W-VB and JS-VB, we use the critic network of input-output dimensionality $(d_X + d_{\theta}, 256, 256, 1)$, the generator network of input-output dimensionality $(d_X + d_Z, 256, 256, d_{\theta})$ and the discriminator network of input-output dimensionality $(d_X + d_{\theta}, 512, 512, 512, 1)$. In addition, both are trained on a reference table of size $T = 50\,000$ simulated under the prior $\tilde{\pi}(\theta)$ learned in the pilot run from B-GAN-2S in Algorithm 2 with a batch size of $B = 1\,280$ and a learning rate $\text{lr} = 10^{-4}$ with 1 000*

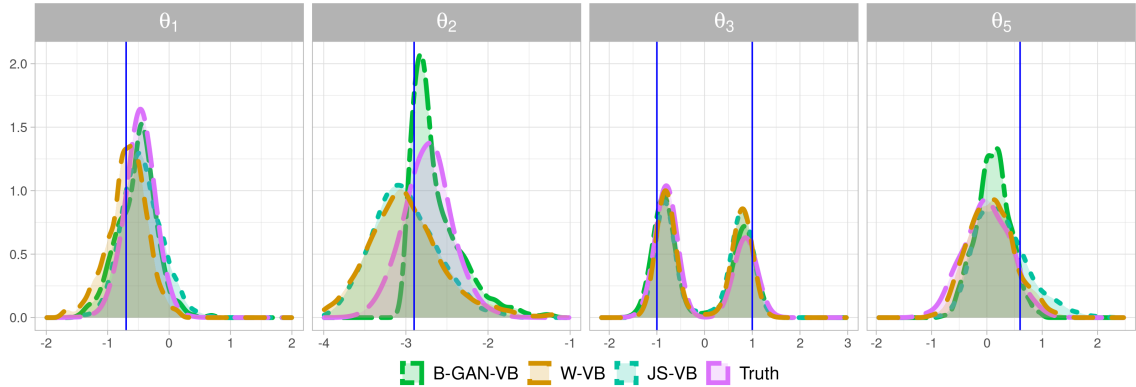


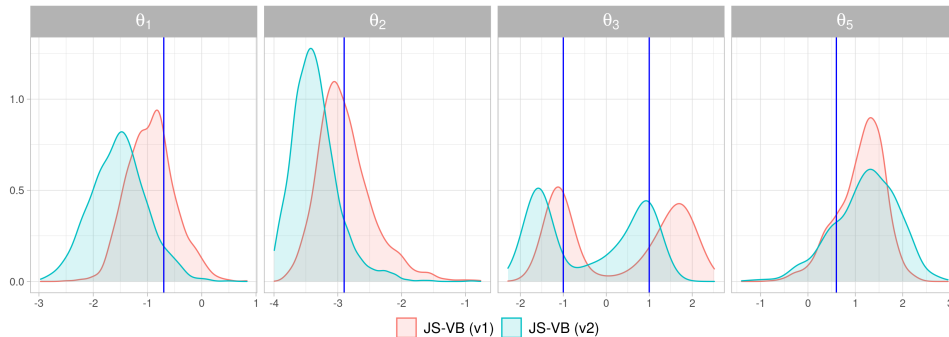
Figure 7: Variational posterior densities under the Gaussian model. The true parameter is $\theta_0 = (-0.7, -2.9, -1.0, -0.9, 0.6)'$.

epochs. We purposely choose a wider and deeper architecture for the discriminator to prevent it from learning faster than the other two. For W-VB, we make $n_\omega = 10$ updates for the critic f_ω , $n_\phi = 5$ updates for the discriminator d_ϕ before we make one update $n_\beta = 1$ for the generator g_β . A typical snapshot of the approximated posteriors under these two implementations and the B-GAN-VB in Algorithm 3 is reported in Figure 7. The summary statistics averaged from 10 repetitions are provided in Table 3. JS-VB provides the tightest CI on average, while B-GAN-VB and W-VB are better at identifying the modes of θ_3 and θ_4 . B-GAN-VB also shows exceptional advantage in learning θ_2 . Additionally, B-GAN-VB is the most robust among the three adversarial VB variants in terms of training. We provide some discussion below.

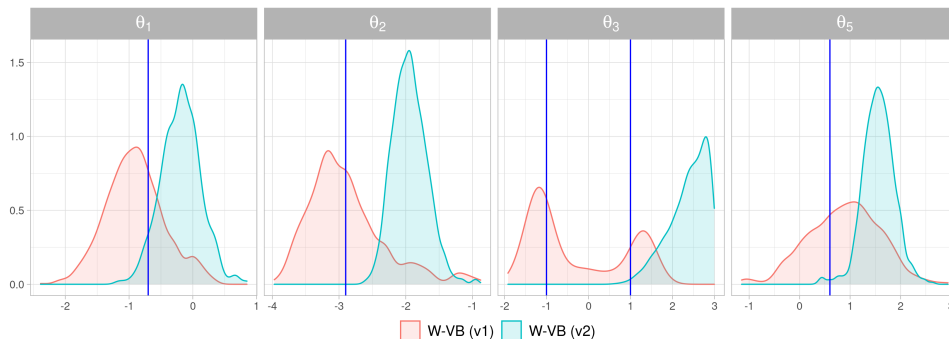
Despite the seemingly promising performance of JS-VB and W-VB, their convergence is contingent on the fragile balance between the networks, due to the unbounded nature of log loss for the discriminator. We see that with mild modifications of the hyper-parameters, the training process can be broken due to zero division, or divergence. A simple illustration is shown in Figure 8. With even slightest modifications, the variational posteriors returned from the generator may deviate a lot. Thus, we recommend B-GAN-VB which appears more robust.

	$\theta_1 = 0.7$		$\theta_2 = -2.9$		$ \theta_3 = 1.0$		$ \theta_4 = 0.9$		$\theta_5 = 0.6$	
	bias	CI width	bias	CI width	bias	CI width	bias	CI width	bias	CI width
Truth	0.63	1.50 (0.8)	0.39	1.04 (0.9)	0.37	2.85	0.27	2.39	0.83	1.68 (0.8)
B-GAN-VB	0.55	1.79 (0.8)	0.19	1.24	0.28	3.03	0.24	2.82	0.55	1.79 (0.9)
JS-VB	0.57	1.43 (0.8)	0.39	1.24 (0.9)	0.34	2.84 (0.9)	0.32	2.12 (0.8)	0.51	1.40 (0.9)
W-VB	0.50	1.97	0.39	1.80 (0.9)	0.29	3.11 (0.8)	0.24	3.07	0.58	1.99 (0.9)

Table 3: Summary statistics of the variational posteriors under the Gaussian model (averaged over 10 repetitions). For θ_3 and θ_4 , we compute the statistics using the absolute values of the parameters, since the posteriors have symmetric modes. Truth refers to the posterior calculated from the exact likelihood function. Bold fonts mark the best model of each column (excluding the true posterior). The coverage of the intervals are 1 unless otherwise stated in the parentheses.



(a) JS-VB



(b) W-VB

Figure 8: Variational posterior densities when the training hyper-parameters change. In both plots, (v1) refers to the configurations used in Figure 7. For JS-VB (v2), we modify the batch size to $B = 5000$ and train for 2000 epochs. For W-VB (v2), we only change the batch size to $B = 2560$ and train for 2000 epochs.

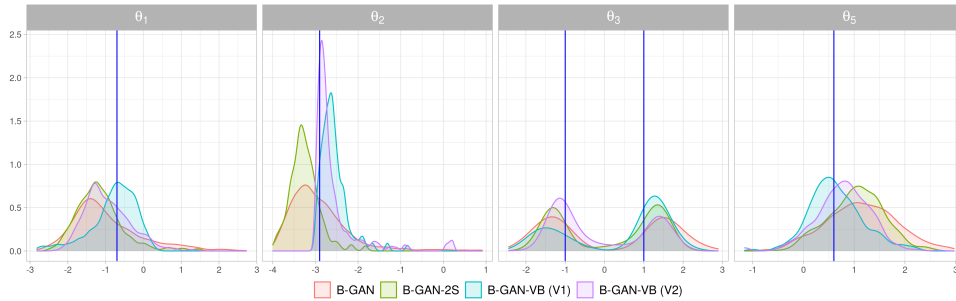


Figure 9: Posteriors from B-GAN-VB under different initializations. V1 is initialized at networks returned from B-GAN, and V2 is initialized at networks returned from B-GAN-2S.

B.3 B-GAN-VB at Different Initializations

We look into the impact of initialization on the VB implementations. The VB updates serve as a local enhancement targeting specifically the neighborhood around X_0 . We consider multiple ways to initialize the critic network and the generator network for B-GAN-VB: (1) zero-weight initializations for both critic and generator networks i.e., $\omega^{(0)} = 0, \beta^{(0)} = 0$; (2) critic network initialized at $\omega^{(0)} = 0$, generator network initialized at a well-trained critic network returned from a previous model (we discuss what this previous model should be below); (3) both critic network and generator network initialized at well-trained networks returned from a previous model. We find that the combination of randomly-initialized critic network and a well-calibrated generator network works well in practice. This is supported by findings in the literature (Stanczuk et al., 2021). Thus, for the rest of the analysis, we initialize the critic function at zero weights, but the generator from a more mature solution.

We now focus on discussing the impact of where the generator gets initialized. Regarding the pre-trained generator, we have two options: (1) the networks returned from B-GAN in Algorithm 1 (V1); (2) the networks returned after the 2-step refinement from B-GAN-2S in Algorithm 2 (V2). We provide the posteriors returned from the two initializations under the Gaussian model in Figure 9, and the summary statistics averaged over 10 repetitions in Table 4. From the results, we observe that both VB versions are able to improve on the performance of the generator that they get initialized at. Not surprisingly, B-GAN-VB

	$\theta_1 = 0.7$		$\theta_2 = -2.9$		$ \theta_3 = 1.0$		$ \theta_4 = 0.9$		$\theta_5 = 0.6$	
	bias	CI width	bias	CI width	bias	CI width	bias	CI width	bias	CI width
B-GAN	0.69	2.89	0.43	2.08	0.37	3.54	0.29	3.12	0.87	2.38 (0.8)
B-GAN-VB (V1)	0.67	2.53 (0.9)	0.49	2.29 (0.8)	0.31	3.31 (0.9)	0.26	2.84	0.38	2.46
B-GAN-2S	0.57	1.73 (0.8)	0.32	1.18 (0.9)	0.28	2.76 (0.8)	0.20	2.30 (0.9)	0.73	1.79 (0.8)
B-GAN-VB (V2)	0.55	1.79 (0.8)	0.19	1.24	0.28	3.03	0.24	2.82	0.55	1.79 (0.9)

Table 4: Summary statistics of the approximated posteriors under the Gaussian model (averaged over 10 repetitions). For θ_3 and θ_4 , we compute the statistics using the absolute values of the parameters, since the posteriors have symmetric modes. Truth refers to the posterior calculated from the exact likelihood function. The coverage of the intervals are 1 unless otherwise stated in the parentheses.

(V2) provides better estimates with smaller biases and tighter credible intervals since it gets initialized at better generator networks returned from B-GAN-2S. We use V2 in our analysis elsewhere in the paper.

C Jensen-Shannon Version of B-GAN

The empirical version of the minimax game using (4) involves the ABC reference table $\{(\theta_j, X_j)\}_{j=1}^T$ and noise realizations $\{Z_j\}_{j=1}^T \sim \pi_Z(\cdot)$ to solve

$$(g^*, d^*) = \arg \min_{g \in \mathcal{G}} \max_{d \in \mathcal{D}} \left(\sum_{j=1}^T \log d(X_j, \theta_j) + \sum_{j=1}^T \log \left[1 - d(X_j, g(Z_j, X_j)) \right] \right). \quad (47)$$

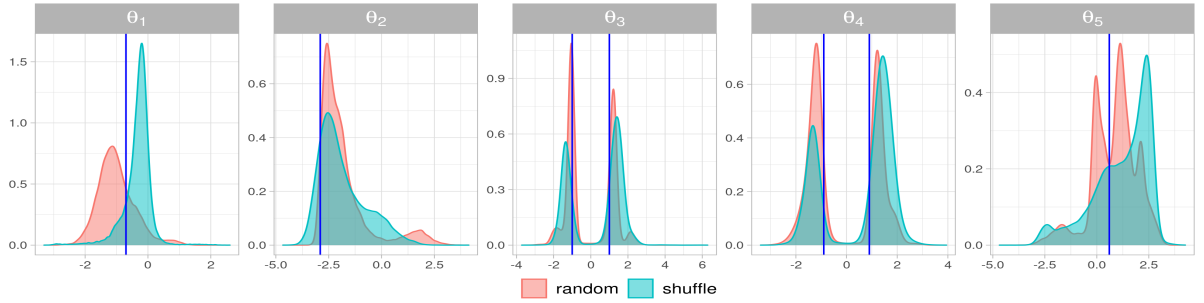
The convergence difficulties of Jensen-Shannon (JS) GANs (Goodfellow et al., 2014), similar to Algorithm 4, have been no secret. We provide a simple illustration of how it can fail on the toy example in Example 1. In particular, we show that the convergence is very sensitive to the choice of the learning rate (step size in stochastic gradient descent). To make comparisons with the Wasserstein version more fair, we use the same network architecture used for Algorithm 1 described in Appendix D.1 for the JS version as well. At the end of this section we point out that JS can work with more careful tuning at higher computational cost.

Algorithm 4 *B-GAN (Jensen-Shannon Version)*

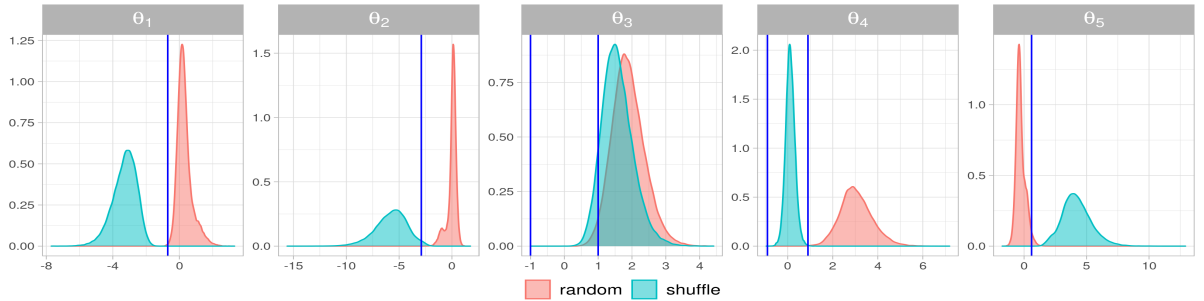
INPUTPrior $\pi(\theta)$, observed data X_0 and noise distribution $\pi_Z(\cdot)$ **PROCEDURE**Initialize networks $d^{(0)}$ and $g^{(0)}$ **ABC Reference Table**For $j = 1, \dots, T$: Generate (X_j, θ_j) where $\theta_j \sim \pi(\theta)$ and $X_j \sim P_{\theta_j}^{(n)}$.**GAN Training**For $t = 1, \dots, N$:Generate noise $Z_j \sim \pi_Z(z)$ for $j = 1, \dots, T$.Update $d^{(t)}$ and $g^{(t)}$ using stochastic gradient descent applied to (47).**POSTERIOR SIMULATION**For $i = 1, \dots, M$: Simulate $Z_i \sim \pi_Z(z)$ and set $\tilde{\theta}_i = g^{(N)}(Z_i, X_0^{(n)})$.

One of the most common causes of failure is an overly-powerful discriminator. Because of the ‘log loss’, when the discriminator learns too fast and becomes too strong, the ‘close-to-boundary’ predictions (near 0 for fake data or near 1 for real data) cause vanishing gradients for the generator. We show how the training balance (between the generator and the discriminator) can be easily disturbed when we alter the learning rate of the generator. We consider two scenarios where the noise variables $\{Z_j\}_{j=1}^T$ are (a) refreshed for each stochastic gradient step, and (b) when they are sampled only once ahead of time and then random minibatches selected for each stochastic gradient steps. In Figure 10, we report the four approximated posteriors for these two scenarios considering two learning rates of the generator (weak $\text{lr}_g = 10^{-4}$ versus strong $\text{lr}_g = 10^{-3}$) while keeping the learning rate of the discriminator at 10^{-4} . When the generator is weak compared to the discriminator ($\text{lr}_g = 10^{-4}$), the posterior reconstructions are not quite around the true values (bottom figure). When the generator is stronger ($\text{lr}_g = 10^{-3}$), the posteriors at least cover the correct locations of the parameters, but they are not nearly as successful as the Wasserstein B-GAN reconstructions we have seen in Figure 1. It is also interesting to compare the results for the two treatments of the noise Z . Sampling Z ’s ahead of time and then sub-sampling for stochastic gradient yields less satisfactory reconstructions.

The JS version of B-GAN could work with a more delicate calibration and exten-



(a) $\text{lr}_g = 10^{-3}$



(b) $\text{lr}_g = 10^{-4}$

Figure 10: Approximated posteriors under different generator learning rates and different Z randomizations. The learning rate of the discriminator is fixed at 10^{-4} in both. The blue vertical lines mark the correct locations of the parameters.

sive training. The Gaussian example was also studied in [Ramesh et al. \(2022, Section 3.1\)](#), who constructed much bigger and deeper networks for both the discriminator and generator. They used a 4-layer network for the generator, with layer widths equal to $(d_X + d_Z, 128, 128, 128, 128, d_\theta)$, and a 5-layer network for the discriminator, with layer widths $(d_X + d_\theta, 2048, 2048, 2048, 2048, 2048, 1)$. They used leaky ReLU activations with a 0.1 negative slope. Using 100 000 pairs of (X_i, θ_i) (twice as many compared to what we used), the networks were trained for 20 000 epochs with 100 discriminator updates per each generator update. Spectral normalization is also applied to ensure stable training. Yet, the authors observed that the performance on the Gaussian example is inferior to SNL (Figure 2A in their paper). Our Wasserstein B-GAN implementation could outperform SNL with much simpler networks, smaller ABC reference table and significantly lower optimization costs. We explored other structures, which are different from the ones mentioned above

and simpler than the ones used by the authors. For example, a generator network with input-output dimensionality as $(d_X + d_Z, 128, 128, 128, d_\theta)$ and a discriminator network with input-output dimensionality as $(d_X + d_\theta, 512, 512, 512, 512, 1)$. However, they did not produce satisfactory posterior approximations.

D Implementation

D.1 Implementation Details for the Gaussian Example

	$\theta_1 = 0.7$		$\theta_2 = -2.9$		$ \theta_3 = 1.0$		$ \theta_4 = 0.9$		$\theta_5 = 0.6$	
	bias	CI width	bias	CI width	bias	CI width	bias	CI width	bias	CI width
Truth	0.63	1.50 (0.8)	0.39	1.04 (0.9)	0.37	2.85	0.27	2.39	0.83	1.68 (0.8)
SNL	0.73	3.50	0.49	2.38	0.40	4.11	0.28	3.47	0.88	3.33
SS	1.25	5.35	1.48	6.53	0.83	5.66	0.86	5.67	1.56	5.69
W2	1.14	3.74	0.98	3.29 (0.9)	0.46	4.20	0.45	3.70	1.36	5.52
	ReLU activations									
B-GAN	0.69	2.89	0.43	2.08	0.37	3.54	0.29	3.12	0.87	2.38 (0.8)
	Architecture (128, 128, 128)									
B-GAN-2S	0.57	1.86 (0.8)	0.32	1.15 (0.9)	0.31	2.91 (0.9)	0.23	2.42 (0.9)	0.84	2.16 (0.8)
B-GAN-VB	0.56	1.96 (0.8)	0.31	1.28 (0.9)	0.33	3.14 (0.9)	0.22	2.56 (0.9)	0.86	2.57 (0.8)
	Architecture (256, 256)									
B-GAN-2S	0.57	1.73 (0.8)	0.32	1.18 (0.9)	0.28	2.76 (0.8)	0.20	2.30 (0.9)	0.73	1.79 (0.8)
B-GAN-VB	0.55	1.79 (0.8)	0.19	1.24	0.28	3.03	0.24	2.82	0.55	1.79 (0.9)
	Leaky ReLU activations									
B-GAN	0.64	2.74	0.39	1.92	0.35	3.53	0.26	3.04	0.86	2.28 (0.8)
B-GAN-2S	0.53	1.77 (0.8)	0.30	1.12 (0.9)	0.33	2.98	0.27	2.52	0.83	2.12 (0.9)
B-GAN-VB	0.53	1.69 (0.8)	0.29	1.13 (0.9)	0.31	2.98 (0.9)	0.19	2.40	0.76	1.95 (0.8)

Table 5: Summary statistics of the approximated posteriors under the Gaussian model (averaged over 10 repetitions). For θ_3 and θ_4 , we compute the statistics using the absolute values of the parameters, since the posteriors have symmetric modes. Truth refers to the posterior calculated from the exact likelihood function. Bold fonts mark the best model of each column (excluding the true posterior). The coverage of the intervals are 1 unless otherwise stated in the parenthese.

Network Architectures. Our implementation of Algorithm 1 in python builds on the codes provided by (Athey et al., 2021).¹¹ We use fairly modest generator/critic networks. For the generator network, we use only 3 hidden layers totaling in dimensions $(d_Z + d_X, 128, 128, 128, d_\theta)$. For the critic network, we use a similar architecture with layer dimensions equal to $(d_\theta + d_X, 128, 128, 128, 1)$. A small amount of regularization (dropout = 0.1 for each layer) was applied to avoid over-fitting. All the weights are initialized at 0 and the $\pi_Z(\cdot)$ is specified as the mean zero Gaussian with identity covariance matrix, dimension d_Z equal to d_θ .

For the post-processing enhancements in Algorithm 2 and Algorithm 3, we choose shallower but wider networks with the hope that they will better capture local aspects (Chen and White, 1999). In particular, for both the generator and critic networks, we use only two-layer networks, resulting in layer dimensions $(d_Z + d_X, 256, 256, d_\theta)$ for the generator and $(d_\theta + d_X, 256, 256, 1)$ for the critic. We summarize comparisons of this setting with the previous 3 layers of 128 units for B-GAN-2S and B-GAN-VB in Table 5. From the results, we see that wider and shallower networks are superior to the deeper and narrower ones for the two local refinements. We have thereby reported posteriors with two layers of 256 units networks in the main paper. In terms of activation functions, our previous analyses are conducted with a ReLU activation, given its expressibility and inherent sparsity (Goodfellow et al., 2016). We have also considered the leaky ReLU with a negative slope $a = 0.1$ (see Table 5) and found no significant advantage of one versus the other. We report results for ReLUs in Figure 1.

Hyperparameters. Regarding the choice of T , for our ABC methods (with summary statistics and the Wasserstein distance), we use a reference table of size $T = 100\,000$. We construct approximated posteriors using the top 1% draws with the smallest ABC discrepancies. For Algorithm 1, we use the same reference table. However, for the stochastic gradient descent updates we use a batchsize $T = 6400$ (implementations in (Ramesh et al., 2022) suggest a batch size around 10% of the total sample size T). The data pairs (X_j, θ_j)

¹¹<https://github.com/evanmunro/dswgan-paper>

are thus subsetting with replacement (not re-sampled) for each iteration of the stochastic gradient descent. The noise variables Z_j 's, however, are refreshed (not pre-sampled and subsetting) for each batch. This is commonly used in existing GAN implementations, including (Athey et al., 2021). We also considered another way of generating the noise variables, where we generate a reference table of $\{Z_j\}_{j=1}^T$ in advance and then re-draw each batch from this set for each epoch. We include a comparison of the posteriors under different noise generating schemes in Figure 11. We observe a bias-variance tradeoff, especially for θ_1 and θ_2 . To avoid the extra bias produced by the pre-fixed noise variable reference table, we refresh Z_j 's for each batch in our analysis. We set $n_{\text{critic}} = 15$, $\lambda = 5$, and the learning rate for the two networks as $\text{lr}_g = \text{lr}_c = 10^{-4}$, which are used in both (Gulrajani et al., 2017) and (Athey et al., 2021). For optimization, we use the ADaptive Moment estimation algorithm (ADAM) by (Kingma and Ba, 2014). We train B-GAN for $N = 1\,000$ epochs or until convergence (the test loss stops decreasing).

For Algorithm 2 and 3, we use smaller reference tables ($T = 50\,000$) with a smaller batch-size 1280, again training the networks for $N = 1000$ epochs. We increase the n_{critic} and the penalty λ with the hope that a regularized and stabilized critic could help the generator to learn better in the local region. In general, a well-behaved critic network always helps but the extra training costs could be high when the sample size is large. Since these local enhancement variants are trained on a smaller reference table, we make these alterations so that they can converge faster with only a minor increase in computation costs. In addition, unlike the JS version of GAN as described in Algorithm 4, the Wasserstein version is less sensitive to the choice of hyper-parameters. Essentially, different hyper-parameters yield similar results and only lead to a trade-off between the convergence speed and computation costs.

Details of Other Methods. For the SNL model (Papamakarios et al., 2019), we adopt the configurations suggested by the authors.¹² They generated 1 000 pairs of (θ_j, X_j) in each round, with 5% randomly selected to be used as a validation set. They stopped training

¹²The authors provide their implementations on <https://github.com/gpapamak/snl>

if the validation log likelihood did not improve after 20 epochs. They suggested 40 rounds for the Gaussian model. Each Masked Autoregressive Flow (MAF) network has two layers of 50 hidden units with hyperbolic tangent function (tanh) activations.

For ABC methods, we use the mean and variance as summary statistics for naive ABC (SS) and the Wasserstein version is implemented using the 2-Wasserstein (W2) distance under the Euclidean metric defined as $W2(X_i, X_j) = \min_{\gamma} \left[\sum_{k_1=1}^n \sum_{k_2=1}^n \gamma_{k_1 k_2} \|X_{i, k_1} - X_{j, k_2}\|^2 \right]^{1/2}$ s.t. $\gamma \mathbf{1}_n = \mathbf{1}_n, \gamma \mathbf{1}_n = \mathbf{1}_n$ with $0 \leq \gamma_{k_1 k_2} \leq 1$. Note that when we calculate the 2-Wasserstein distance, each X_i is treated as 4 pairs ($n = 4$) of bi-variate normal variables rather than a flat vector of length 8. For both methods, the approximated posteriors are constructed using the ABC draws with the top 1% smallest data discrepancies. Performance details (after 10 repetitions) are summarized in Table 5.

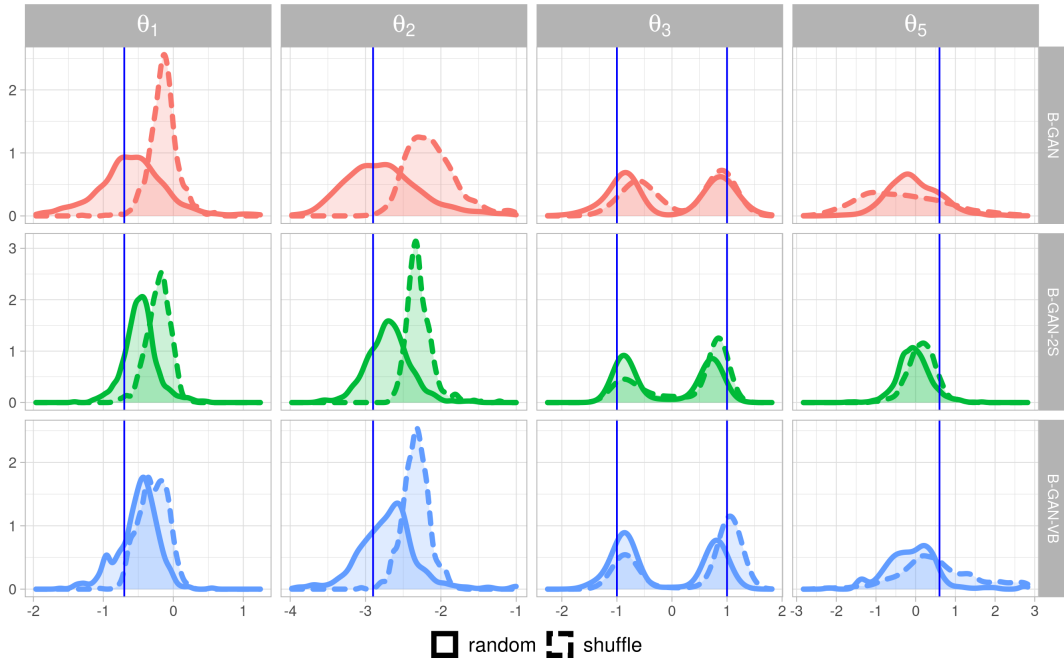


Figure 11: Approximated posteriors under different noise variable refresh strategies.

D.2 Implementation Details for the Lotka-Volterra Example

We adopt wider networks for the Lotka-Volterra example given the challenge of learning from higher dimension of the covariates ($q = 402$). For Algorithm 1 (under the orig-

inal uniform prior), we use ReLU neural networks with $L - 1 = 3$ hidden layers with (256, 256, 128) units from bottom to top for both the generator and the critic functions. We generate $T = 1\,000\,000$ pairs of (X_i, θ_i) for the vanilla B-GAN, and the networks are trained with a batch size $B = 12\,800$ for 1 000 epochs. We adopt the same $n_{\text{critic}}, \lambda, \text{lr}_g = \text{lr}_c$ as the Gaussian example in Appendix D.1.

For learning from the adjusted prior $\tilde{\pi}(\theta) = \pi_{\hat{g}}(\theta | X_0)$ where \hat{g} was obtained from Algorithm 1, we choose shallower networks with $L - 1 = 2$ hidden layers and $W = 256$ hidden units in each layer. We generate $T = 50\,000$ samples for local enhancements and use a batch size $B = 1\,280$ for training. For the VB variant (B-GAN-VB in Algorithm 3), we initialize the generator at $g_{\hat{\beta}}$ and the critic at $f_{\hat{\omega}}$ returned from B-GAN-2S in Algorithm 2.

For the two ABC methods, we use the same $T = 1\,000\,000$ pairs used in the B-GAN training. We adopt the summary statistics described in Section 5.1 for the naive ABC (SS) and Wasserstein version is calculated on top of the pairs of predator-prey population $\{x_t, y_t\}$. For both models, we again accept ABC draws with the top 1% smallest data discrepancies.

For the SNL model, the author suggested building the network on top of the same set of summary statistics used in naive ABC, and 20 epochs of training. The network architecture and other training configuration remain the same as in Appendix D.1.

D.3 Implementation Details for the Boom-and-Bust Example

We generate $T = 500\,000$ pairs of (X_i, θ_i) for training the vanilla B-GAN in Algorithm 1. We use the same batch size, learning rate and network architectures as in Appendix D.1, except that we train the networks for 2 000 epochs this time. We have explored three types of different inputs: (1) the time-series itself; (2) the summary statistics suggested by previous literature such as (An et al., 2020) (described in Section 5.2); (3) the time-series together with the summary statistics. We find the one built on only the summary statistics works best.

For the local enhancement variants, B-GAN-2S in Algorithm 2 and B-GAN-VB in

Algorithm 3, we generate $T = 50\,000$ samples. The network architectures and training configurations are the same as the ones in Appendix D.1.

For ABC methods, they are built on the same $T = 500\,000$ draws used in B-GAN. We adopt the summary statistics mentioned in Section 5.2 for the naive ABC (SS), and the 2-Wasserstein ABC is trained on the time series.

For SNL models, we use the summary statistics as the input to the networks and train the model for 20 epochs, similar to the setting used in Appendix D.2.

D.4 Implementation Details for the Heston example

We use the same reference sizes and training configurations as described in Appendix D.3 for B-GAN, B-GAN-2S and B-GAN-VB. Besides the time-series itself, we add the following summary statistics (which are sufficient for an observable AR(1) process) to the data

$$s_1 = \sum_{t=2}^{n-1} y_t, s_2 = \sum_{t=2}^{n-1} y_t^2, s_3 = \sum_{t=2}^n y_t y_{t-1}, s_4 = y_1 + y_n, s_5 = y_1^2 + y_n^2. \quad (48)$$

For AL, we follow Martin et al. (2019) and generate a reference table of size $T = 111\,803$ and $T = 894\,427$ for $n = 500$ and $n = 2\,000$ (guided by the theoretical results in Frazier et al. (2018)). The reference table size is $T = 331\,882$ for the real data analysis. The details of the implementation can be found in Martin et al. (2019).

For SNL, we use the concatenation of time series and its summary statistics in (48) as the input to the networks. The model is trained for 30 epochs, using the same training configurations as Appendix D.1.

D.5 Computation Costs Comparison

We provide comparisons of computation times of each method in Table 6 for the Gaussian example and the Lotka-Volterra model. Note that SS, W2 and SNL were executed with CPUs and all B-GAN models were computed using GPUs. We report the time of B-GAN-2S and B-GAN-VB for computation using the adjusted prior only (i.e. without the pilot run). Since B-GAN model learns the joint distribution of (X, θ) and is universal regardless of the

observed data X_0 , we recycle the same pre-trained B-GAN model to recover the adjusted prior repeatedly for different X_0 in our simulation study. Although we only report the computation time for one repetition here, this feature saves a lot of computation costs when one wants to investigate average performance from multiple repetitions.

The complexity of computing the exact Wasserstein distance is $\mathcal{O}(T^3)$ (Burkard et al., 2009) and $\mathcal{O}(T^2)$ (Cuturi, 2013) for the approximate one. The computation costs of SNL and B-GAN depends on the network architecture and how fast the networks converge. We can only give a rough computation complexity estimate as $\mathcal{O}(T \times \#epochs \times \#weights)$ for these neural network based models. From Table 6, we observe that our methods could be more scalable than W2 and SS when the dimension of the dataset is high (8 of Gaussian model vs 402 of Lotka-Volterra (LV) model). The computation time of SNL on LV is smaller than for the Gaussian model due to fewer epochs in training (the author suggested 20 rounds for LV and 40 rounds for Gaussian model). In addition, SNL is trained on summary statistics ($q = 9$) rather than the time-series for the LV model. The computation costs of SS increase significantly on the LV example, resulting from both the increase in dimension and the computation costs of the selected summary statistics. The computation costs of the Wasserstein distance are unsurprisingly high as it is known that they do not scale well.

	SS	W2	SNL	B-GAN	B-GAN-2S	B-GAN-VB
Gauss	33.75	221.28	4790.56	2736.93	676.25	726.22
Lotka-Volterra	5846.95	162644.96	3080.96	1610.05	762.21	753.61

Table 6: Computation time of one repetition for each method on Gauss example and Lotka-Volterra (LV) example (in seconds). The time of B-GAN-2S and B-GAN-VB is for computation using the adjusted prior.